2013-09-13

Numerical Modeling of Pipe-Soil Interaction under Transverse Direction

Farhadi Hikooei, Bahar

UNIVERSITY OF CALGARY

Numerical Modeling of Pipe-Soil Interaction under Transverse Direction

by

Bahar Farhadi Hikooei

A THESIS

SUBMITTED TO THE FACULTY OF GRADUATE STUDIES
IN PARTIAL FULFILMENT OF THE REQUIREMENTS FOR THE
DEGREE OF MASTER OF ENGINEERING

DEPARTMENT OF CIVIL ENGINEERING

CALGARY, ALBERTA

AUGUST, 2013

Abstract

Based on Winkler method, pipe can be simplified as a beam, while pipe-soil interaction can be represented by soil springs in the axial, horizontal and vertical direction. Pipe deflection and resultant forces are related to each other by coefficient K in the equation $F=K\delta$, where F is the resultant force and δ is the pipe displacement. This project studies pipe-soil interaction for pipelines buried in clay and sand subjected to pipeline displacement in oblique direction. The objective is to quantify the effect of soil parameters on coefficient K and maximum soil resistance. Pipe-soil behavior has been studied using the finite element software ABAQUS/CAE. There were totally 48 models with varying soil parameters, pipe burial depth and pipe-soil interaction friction to investigate the effect of each variable on pipe-soil behavior. The results have been presented in normalized force-displacement plots to identify the parameters which affect the soil resistance most. In addition they have been compared to the analytical results from ALA (2001) and proposed failure envelopes in previous studies. The results show that the maximum normal force per unit length depends on the type of soil surrounding the pipe. By comparing all the results pipe burial depth, soil cohesion, friction and dilation angles were found to have a significant effect on pipe-soil interaction and can considerably increase the maximum soil resistance.

Acknowledgements

I wish to express my sincere thanks to my supervisor Dr. R.C. Wong for his guidance throughout this research. I am really grateful to Dr. Wong for all his patience, guidance and suggestions during my master program.

I would like to extend my appreciations to my professors at University of Calgary during my master program. That was a great chance for me to attend their classes.

Finally, I would like to thank my husband who was always with me in all hard times, my parents who always supported me by their words, I owe all my life to you, and my parents in-law who were by me in my loneliness.

Table of Contents

Abstract.....ii
Acknowledgements iii
Table of Contents.....iv
List of Tables.....vi
List of Figures and Illustrations vii
Chapter 1: Introduction to Pipeline Modeling..... 1
1.1 Introduction..... 1
1.2 Literature review..... 3
1.3 Winkler method..... 6
1.4 ALA guideline..... 7
1.5 Failure criteria..... 10
Chapter 2: Finite Element Modeling..... 13
2.1 Numerical modeling procedure..... 13
2.2 Pipe modeling..... 15
2.3 Soil modeling..... 15
2.4 Interface..... 16
2.5 Modeling steps..... 17
2.6 Modeling cohesive materials (clay)..... 19
2.7 Modeling frictional material (sand)..... 19
Chapter 3: Results and Discussions..... 25
3.1 Behavior in cohesive material (clay)..... 25
3.2 Behavior in frictional material (sand)..... 29
3.2.1 Effect of pipe burial depth..... 30
3.2.2 Effect of inclination angles..... 31
3.2.3 Effect of sand friction angle..... 33
3.2.4 Effect of sand dilation angle..... 35
3.2.5 Effect of pipe-soil friction angle..... 37
3.2.6 Effect of in-situ stress coefficient..... 37
3.2.7 Linear elastic case versus elasto-plastic case..... 38

3.2.8 Superimposition of effects..... 39

3.2.9 Yield surface and Failure envelope..... 40

3.3 Surface heave..... 43

Chapter 4: Conclusion..... 65

4.1 Conclusion..... 65

4.2 Recommendation for future studies..... 66

References 67

Appendices A: Symbols..... 69

Appendices B: Lateral Bearing Capacity Factor of Soil (ALA2001)..... 71

List of Tables

Table 1. Input parameters in modeled cases:……21
Table 2. Effect of pipe displacement angle (α) on clay maximum resistance (C_u=35 kPa, H/D=3.03)……45
Table 3. Comparison of vertical and horizontal bearing capacity factors estimated from ALA (2001) and finite Element modeling (C_u=45 kPa, H/D=3.03, α=0°)……45
Table 4.Comparison of vertical and horizontal soil resistance estimated from ALA(2001) and finite element modeling (C_u=45 kPa, H/D=3.03, α=0°)……45
Table 5. Effect of pipe displacement angle (α) on sand maximum resistance (H/D=3.03, φ=35° and Ψ=10°)……46
Table 6. Effect of friction angle on plastic deformation (H/D=3.03, Ψ=10°and α=0°)……46
Table 7.Maximum sand resistance for varying Ko (H/D=3.03, φ =35°, Ψ=10°, α=0°)……46
Table 8. Sand surface Heave for varying Ko (H/D=3.03, φ =35°, Ψ=10°, α=0°)……46
Table 9. Comparison between the effect of dilation angle and pipe displacement angle on maximum resistance in sand for H/D=3.03 and φ =35°……47
Table 10. Comparison between the effect of friction angle and pipe burial depth on maximum resistance in sand for pipe vertical displacement (α=0°) and Ψ=10°……47
Table 11.Comparing effect of different displacement angle on horizontal and vertical maximum resistance in sand for H/D=3.03, φ =35° and Ψ=10°……47
Table 12. Comparing the effect of different displacement angles and pipe burial ratio on maximum resistance in sand for φ =35° and ψ =0° ……47
Table 13.Comparing the effect of pipe-soil friction coefficient on maximum resistance in sand for H/D=3.03, φ =35° and ψ=10°……48
Table 14.Comparision between bearing capacity factors and soil maximum resistance estimated ALA(2001) and finite element modeling in sand……48

List of Figures and Illustrations

Figure 1.Springs in BNWF model representing soil resistance (ALA, 2001) 12
Figure 2 Schematic showing pipe-soil interaction, boundary conditions, and displacement angle 23
Figure 3 Finite element mesh for pipe-soil interaction: a) Base model with 1996 elements for soil, and b) Refined finite element mesh with 2453 elements for soil 23
Figure 4 Mesh convergence study 24
Figure 5 Dependency of force-displacement responses on pipe displacement angle for H/D=3.03, Cu=45 kPa, for total soil resistance, a) FEM results, and b) Guo (2005) 49
Figure 6 Dependency of force-displacement responses on pipe displacement angle for H/D=3.03, Cu=45 kPa, for the horizontal component of soil resistance a) FEM results, and b) Guo (2005) 50
Figure 7 Dependency of force-displacement responses on pipe displacement angle for H/D=3.03, Cu=45 kPa, for the vertical component of soil resistance a) FEM results, and b) Guo (2005) 51
Figure 8. Deformed finite element mesh as a result of pipe vertical displacement of δ/D=0.3, α=0°, (C_u=45 kPa, H/D=3.03), Displacement contours (m) 52
Figure 9. Deformed finite element mesh as a result of pipe oblique displacement of δ/D=0.3, α=45°, (C_u=45 kPa, H/D=3.03), Displacement contours (m) 52
Figure 10 Mobilization of vertical and horizontal resistances in clay for pipe displacement of δ/D=0.2 in different displacement angles (α), H/D=3.03, C_u=35 kPa 53
Figure 11. Normalized force-displacement curves for clay with different cohesion for H/D=3.03 and α=0 53
Figure 12.Effect of pipe burial depth on force-displacement response in sand for φ=35°, Ψ=10°and α=0 54
Figure 13. Deformed finite element mesh as a result of pipe vertical displacement of δ/D=0.5, α=0°, H/D=1.5, φ=35°, and Ψ=10°; Total displacement contours (m) 54
Figure 14. Deformed finite element mesh as a result of pipe vertical displacement of δ/D=0.5, α=0°, H/D=6, φ=35°and Ψ=10°; Displacement contours (m) 55
Figure 15. Deformed finite element mesh showing the plastic zone developed in sand as a result of pipe vertical displacement of δ/D=0.5, H/D= 1.5, φ=35°and Ψ=10°. Plastic strain contours (%). 55
Figure 16. Deformed finite element mesh showing the plastic zone developed in sand as a result of pipe vertical displacement of δ/D=0.5, H/D= 6, φ=35°and Ψ=10°. Plastic strain contours (%) 56
Figure 17. Effect of pipe displacement angle on force-displacement response in sand for H/D=3.03, φ=35°and Ψ=10° 56
Figure 18. Effect of displacement angle on sand horizontal force-displacement response in sand for H/D=3.03, φ=35°and Ψ=10° 57
Figure 19.Effect of loading angle on sand vertical force-displacement response in sand for H/D=3.03, φ=35°and Ψ=10° 57
Figure 20. Sand vertical resistances versus horizontal resistance, H/D=3.03, φ=35°, Ψ=10° 58
Figure 21. Effect of friction angle on force-displacement response in sand for H/D=3.03, Ψ=10°and α=0° 58
Figure 22. Effect of soil dilation angle on force-displacement response in sand for H/D=3.03, φ=35°and α=0° 59

Figure 23. Effect of pipe-soil interface friction on force-displacement response in sand for H/D=3.03, φ=35°, Ψ=10°and α=0° 59
Figure 24. Effect of K_o on sand force-displacement response, H/D=3.03, ϕ=35º, Ψ=20º, α=0º 60
Figure 25. Force-displacement response in elastic and elasto-plastic models, H/D=3.03, α=0° 60
Figure 26. Failure envelope obtained from FEM analysis for different burial depth, compared to the proposed model by Guo (2005a) for ϕ=35º, Ψ=10º 61
Figure 27. Failure envelope obtained from finite element normalized results for different burial depth, compared to the proposed model by Guo (2005a) for ϕ=35º, Ψ=10º 61
Figure 28. Yield surfaces obtained from FEM analysis for different loading surfaces, compared to the proposed model by Guo (2005a), H/D=3.03, ϕ=35º, Ψ=10º 62
Figure 29. Effect of dilation angle and pipe burial depth on surface heave in sand for pipe vertical displacement (α=0°) and φ= 35° 62
Figure 30. Effect of dilation angle and pipe burial depth on surface heave in sand for pipe 45º displacement (α=45°) and φ= 35° 63
Figure 31.Effect of dilation angle and pipe burial depth on surface heave in sand for horizontal pipe displacement (α=90°) and, φ= 35° 63
Figure 32. Effect of dilation angle and pipe burial depth on surface horizontal displacement in sand for pipe displacement of 45º (α=45°), and φ= 35° 63
Figure 33. Effect of dilation angle and pipe burial depth on surface horizontal displacement in sand for pipe horizontal displacement (α=90°), and φ= 35° 63

Chapter One: Introduction to Pipeline Modeling

1.1 Introduction

Pipelines are safe and economical means of transporting gas, water, sewage and other fluids. To provide a better protection and support, buried pipelines are used widely in industry. Many of the existing pipelines are located at shallow depths beneath roads in urban areas and are subjected to a variety of external loads. Failure of an oil and gas pipeline can cause serious economic and environmental consequences, and in some circumstances may lead to gas explosions resulting in loss of human life. Also, large amount of money are being spent annually in repair and replacement of pipelines. In terms of property damage PHMSA (Pipeline and Hazardous material safety administration) records indicate that the 20-year average (1993-2012) cost of significant pipeline incidents is over 318 million dollars, the 10-year average (2003-2012) cost is over 494 million dollars, the 5-year average (2008-2012) cost is over 545 million dollars, and the 3-year average (2010-2012) cost is over 662 million dollars.

In general, significant numbers of pipe damages are a result of induced loads in pipeline that can happen as a consequence of permanent ground deformation, such as earthquakes, slope failure, landslides and liquefaction.

Based on the annual report published by National Energy Board (NEB), 6% of the NEB-regulated pipeline ruptures since 1991, due to geotechnical causes. (NEB, 2009)

To minimize the risk of any accident, injury and material loss and also to prevent the damages that cause a great hazard to the environment, the pipeline industry has been interested in predicting soil and pipe behavior when the pipeline is subjected to external

loadings. Owing to the highly nonlinear behavior of soil material, pipe-soil interface phenomena, and the possibility of pipe distortion, buried pipe-soil system has a relatively complex behavior.

1.2 Literature Review

Audibert & Nyman (1977) used an analytical method to determine the load-displacement curve for buried pipes with different diameters. The analytical results were compared to series of experiments on a small scale pipe model. Later, Nyman (1984) proposed an analytical approach to accommodate the effect of oblique movement of pipes. Using the similarity between the restraint of buried inclined anchor plates and restraint of pipelines subjected to motion in the oblique direction, Nyman (1984) extended the behavior of soil restraint in inclined anchors to buried pipes.

Based on Nyman's equations (Nyman, 1984), the four principal directions of buried pipeline restraint are vertical-uplift, horizontal-lateral, vertical-bearing, and longitudinal-axial. The remaining soil restraint categories out-of-plane with the primary directions are associated with oblique pipe motion. An analogy is made between restraint of buried inclined anchor plates and restraint of pipelines subjected to motion in the horizontal-vertical (lateral-uplift) direction. He proposed design procedures to develop bilinear load-displacement relationship for soil restraint of pipelines subjected to oblique displacement.

Trautmann & O'Rourke (1985) studied the results of an experimental program to assess the response of buried pipes to lateral ground movements considering the effect of pipe depth, pipe diameter, and pipe roughness. A detailed research on buried pipeline published by Guo & Stolle (2005a) studied the pipe-soil interaction for pipes buried in frictional soil when subjected to lateral ground movement. In this study the effect of pipe size and burial depth on pipe-soil peak strength was investigated by introducing a failure surface in the force (or load) space to define the ultimate states of pipe–soil interaction. The process of pipe movements is described by a set of loading surfaces and a plastic

displacement potential that defines the direction of incremental plastic pipe displacements. The evolution of the loading surface, both the dimension and the shape, depends on both pipe displacements and the burial depth ratio. Good agreement is obtained between model predictions and the results of finite element analyses. The proposed failure envelope has been discussed in section 1.5.

Following this study, Guo (2005b) published a study on the behavior of buried pipe in clay under oblique loading. In this publication, the pipe-soil interaction for pipelines subjected to combined horizontal and vertical movements in the oblique direction was studied using finite element modeling. The study reproduced the key features of force-displacement responses obtained from continuum finite element analyses for pipes of different sizes and various burial depth ratios in clay. Another publication by Merifield et al. (2008) focused on the results of finite element analyses of partially buried pipelines under vertical and horizontal load. The results have been compared to the collapse loads calculated using the upper-bound theorem of plasticity. In particular, these analyses examine the influence of separation between the pipe and the soil when tension is applied. Separate yield envelopes are derived for the cases involving separation (no tension) and full bonding (full adhesion / unlimited

tension) at the pipe-soil interface.

Daiyan et al. (2010) studied the effect of displacement angle on the pipe-soil behavior in the horizontal plane. In this experimental study the axial/lateral interaction of pipes in dry sand has been investigated using a series of centrifuged tests of pipelines being displaced

in a horizontal plane. This experimental study shows that using discrete springs system in structural modeling of pipe/soil interaction during axial/lateral pipe/soil movements required coupled soil-spring formulations. Also, Badv & Daryani (2010) studied the effect of pipe burial depth and pipe diameter on the upward and lateral soil-pipeline interaction using finite difference method. Their study results showed that the transverse soil restraint decreases for larger diameter pipes in the horizontal direction, and there is no effect in the vertical direction. The transverse soil restraint increases with increasing burial depth ratio but it becomes constant at deeper soil profiles.

With respect to the role of pipelines in industry and the importance of predicting pipeline behavior, the American Lifelines Alliance (ALA) was formed with the purpose of developing design provisions to evaluate the integrity of buried pipe for a range of applied loads. According to ALA (2001) guideline, soil loading on the pipeline is represented by discrete nonlinear springs (Winkler method), and several equations have been proposed for the maximum soil resistance for buried pipeline in homogenous soil condition. These expressions for the maximum soil spring force are based on laboratory and field experimental investigations on pipeline responses, as well as general geotechnical approaches for related structures, such as piles, embedded anchor plates, and strip footings (ALA, 2001).

Another method used to predict the pipe-soil interaction behavior is the finite element (FE) method, which provides a comprehensive tool for predicting the detailed performance of buried structures. It can take into account the non-linear soil behavior, bedding details, interaction between soil and pipe, and any geometric shape.

In this project the pipe-soil behavior under pipe displacement has been studied using ALA equations, proposed failure criterion and finite element modeling.

The principal objectives of the present project are:

- To study the interaction between pipe and soil under different oblique loading and to identify the parameters that govern the interaction. By modeling pipe-soil interaction using finite element method, the effect of soil parameters on the soil maximum resistance and foundation coefficients in the Winkler model has been studied.
- To validate the existing predictive models developed by ALA (2001) and the proposed failure criteria by Guo (2005). The pipe-soil behavior in different cases has been compared to the force-displacement equations in ALA guidelines and the proposed failure envelopes by varying pipe burial depth, soil cohesion, soil in-situ stress coefficient, pipe-soil interface friction coefficient and soil dilation and friction angles.

1.3 Winkler model

The beam on nonlinear Winkler foundation (BNWF), named as Winkler model is an improved linear spring model and is used for predicting the nonlinear static response of pipe-soil system. (Allotey & El Naggar, 2008)

In the Winkler model the soil-pipe interaction is modeled as a pipe resting on nonlinear soil springs. In 2D modeling, the pipe can be modeled as a beam element and the soil resistance along the pipe as nonlinear springs; there are four groups of springs to model soil and pipe displacements and rotations:

a) Axial soil spring: representing the soil resistance along the pipeline axis.

b) Lateral soil spring: representing the lateral resistance of soil to the pipe transverse movement.

c, d) Vertical bearing spring and vertical uplift spring: representing the vertical resistance of soil at the bottom and at the top of the pipe, respectively.

Figure 1 demonstrates these four groups of springs in Winkler method.

Based on Hooke's law, a linear relationship between the force on the spring foundation (F) and the deflection δ is assumed:

$$F=K.\delta \quad (1.1)$$

The modulus of subgrade reaction, K [F/L], is the ratio between the soil pressure per unit length of pipe, P [F/L], and the displacement produced by the load application at that point, δ.

In this project, since the 2D behavior of pipe-soil interaction has been modeled, the axial soil spring is neglected and the modeling is based on the lateral springs and vertical uplift and bearing springs.

1.4 ALA guideline

The limit theorems are powerful tools for analyzing stability problems in soil mechanics. Limit analysis is a structural analysis field which is dedicated to the development of efficient methods to directly determine estimates of the collapse load of a given structural

model without resorting to iterative or incremental analysis. The limit analysis is based on two limit theorems: Lower and upper bound theorem:

In the lower bound theorem (Static Theorem) an external load computed on the basis of an assumed distribution of internal forces, in which the forces are bounded by limit values, and the forces are in equilibrium, is less than or equal to the true collapse load.

On the other hand in the upper bound theorem (Kinematic Theorem) an external load computed on the basis of an assumed mechanism, in which the forces are in equilibrium, is always greater than or equal to the true collapse load.

With respect to the limit analysis theorems, The American lifeline alliance (ALA) guideline suggests the following equations to estimate the maximum lateral resistance of soil per unit length of pipe:

$$P_u = N_{ch} C_u D + N_{qh} \overline{\gamma} HD \qquad (1.2)$$

where C_u is soil cohesion, D is the pipe diameter, H is the burial depth of the pipeline, and $\overline{\gamma}$ is the effective unit weight of soil. Also, N_{ch} and N_{qh} are the horizontal bearing capacity factors for clay and sandy soils, respectively. They are given as:

$$N_{ch} = a + bx + \frac{c}{(x+1)^2} + \frac{d}{(x+1)^3} \qquad (1.3)$$

$$N_{qh} = a + bx + cx^2 + dx^3 + ex^4 \qquad (1.4)$$

where, x is the pipe burial depth ratio, which is the ratio of depth of the pipeline to the pipe diameter ($x = \frac{H}{D}$).

The values for a, b, c, d and e can be found in design guidelines tables based on friction angle (ALA, 2001). The table for capacity factors is attached in Appendix A.

With respect to equations (1.2) to (1.4), in ALA guidelines, the soil maximum lateral resistance is a function of soil friction angle, cohesion and unit weight and also it is highly related to the pipe burial depth ratio ($\frac{H}{D}$).

Furthermore, the maximum soil resistance per unit length of the pipeline in the vertical uplift can be calculated:

$$Q_u = N_{cv} C_u D + N_{qv} \bar{\gamma} H D \qquad (1.5)$$

where: $N_{cv} = 2(\frac{H}{D})$ (1.6)

$$N_{qv} = (\frac{\phi H}{44D}) \qquad (1.7)$$

By factoring the depth ratio from the above equations

$$Q_u = \frac{H}{D} . \left\{ 2cD + \frac{\phi}{44D} \bar{\gamma} H D \right\} \qquad (1.8)$$

With respect to the equations above, same as the lateral resistance, the soil resistance in the vertical uplift is a function of friction angle, cohesion, and effective unit weight of soil. Also, it is linearly related to the pipe burial depth ratio.

In these equations when the pipes locates on soil surface, x=0, the maximu lateral soil resistance will only have an cohesive component and will become:

$$P_u = a C_u D$$

And the maximum vertical soil resistance will become zero. $Q_u = 0$

1.5 Proposed failure criteria

Nyman (1982) proposed an analytical approach to study the effect of oblique pipe movement on the vertical and horizontal resistance of the soil:

$$f = (\frac{F_h}{F_{uh0}})^2 + \frac{F_v}{F_{uv0}} - 1 = 0 \qquad (1.9)$$

with F_{uh0} and F_{uv0} being the maximum horizontal and vertical forces corresponding to purely horizontal and vertical (upward) pipe movements, respectively. F_h and F_v are the maximum horizontal and vertical soil resistances for a given pipe displacement. These maximum horizontal and vertical forces resulted from pipe purely horizontal or vertical displacement, F_{uh0} and F_{uv0}, have been referenced to as P_u and Q_u in ALA guideline, respectively.

Later, Guo (2005), by comparing the experimental data of Das (1985) and Meyerhof and Hanna (1978), used a modified form of failure criterion for cohesive soil:

$$f = (\frac{F_h}{F_{uh0}})^2 + (\frac{F_v}{F_{uv0}})^2 - 1 = 0 \quad (1.10)$$

He normalized F_{uh0} and F_{uv0} by undrained shear strength of clay and pipe diameter:

$$N_{ch0} = \frac{F_{uh0}}{C_u D} \text{ and } N_{cv0} = \frac{F_{uv0}}{C_u D}, \qquad (1.11)$$

where with respect to equations (1.2) and (1.5), N_{ch0} and N_{ch0} are the horizontal and vertical bearing capacity factors for clay, respectively. For normalizing F_{h0} and F_{v0} in sand, using equations (1.2) and (1.5), we can write:

$$N_{qh0} = \frac{F_{uh0}}{\gamma HD} \quad \text{and} \quad N_{qv0} = \frac{F_{uv0}}{\gamma HD}. \quad (1.12)$$

Furthermore, Guo (2005a) assumed the yield surface under induced oblique loading to have the same functional form as the failure envelope:

$$f_y = F_h{}^2 + (\frac{F_v}{\beta})^2 - F_v{}^2 = 0 \quad (1.13)$$

Where the coefficient β is:

$$\beta = \frac{F_{ho}}{F_{vo}} \quad (1.14)$$

where F_{ho} and F_{vo} are the horizontal and the vertical forces when the pipe undergoes purely horizontal and vertical movement at a given pipe displacement, respectively. (Note that F_{uho} and F_{uvo} are the maximum forces in the horizontal and vertical directions, respectively.)

In this project the application of this failure criterion for sand has been studied. Also, the results from finite element have been compared to those estimated from ALA (2001).

To distinguish between the results from different methods and avoid confusion, in this project the horizontal and the vertical bearing capacity factors calculated from ALA (2001), equations (1.4) and (1.7), are symbolized by N_{qh} and N_{qv}, and the horizontal and the vertical bearing capacity factors from finite element modeling are represented by, $\frac{F_h}{\gamma HD}$ and $\frac{F_v}{\gamma HD}$.

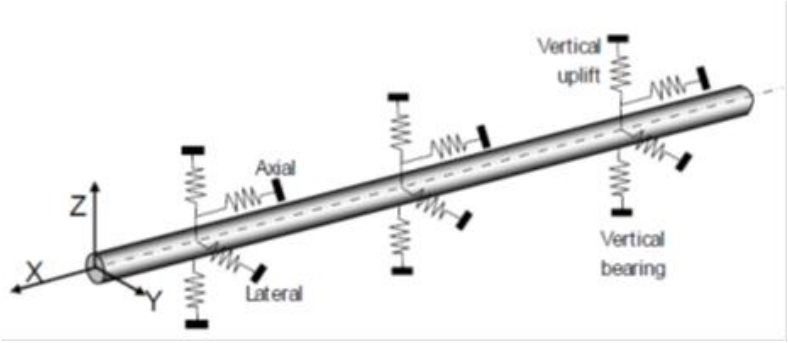

Figure 1.Springs in BNWF model representing soil resistance (ALA, 2001)

Chapter Two: Finite Element Modeling

In modeling the pipe-soil interaction, a number of aspects need to be considered:

- The mechanical behavior of pipeline
- The behavior of the soil surrounding the pipeline
- The interaction between the soil and the buried pipeline.
- The geometry and orientation of the pipeline
- Proper elements for modeling pipe, soil and interface condition

In this project, the soil-pipe behavior has been modeled with a 2D numerical model using finite element software, ABAQUS.

2.1 Modeling procedure

For selecting an appropriate element type for pipe-soil model, several element parameters should be considered:

- Family (continuum, shell, beam, rigid elements,…)
- Degrees of freedom (directly related to the element family)
- Number of nodes
- Formulation
- Integration

A family of finite elements is the broadest category used to classify elements and an example of commonly used element families are: continuum, shell, beam, rigid, membrane and etc. Elements in the same family share many basic features. One of the

major distinctions between different element families is the geometry type that each family assumes.

Among different element families that ABAQUS provides, continuum or solid elements can model the widest variety of components. They simply model small blocks of material in a component and because of their shape they can be connected to other elements on any of their faces and they can be subjected to any loading.

Continuum elements can be used for both linear analysis and also for complex nonlinear analysis, which includes contact, plasticity, and large deformations.

In finite element methods for each element, displacement, rotations, pressure and other degrees of freedom are only calculated at the nodes of the element and they are interpolated between nodes for any other point in the element. This interpolation order depends on the number of nodes on that element.

The elements with nodes only at their corners, use linear or first-order interpolations in each direction and are often called linear elements or first-order elements while elements with mid-side nodes, use quadratic interpolation (second-order interpolation). Second-order elements provide a higher accuracy than first-order elements.

Since first-order elements are stiff and have a small rate of convergence and for using them a very fine mesh is needed, which is not beneficial, they should be avoided as much as possible in stress analysis problems. Consequently second-order elements, which capture stress concentration more effectively, are better choices for modeling geometric features.

The ABAQUS element library includes linear and quadratic interpolation elements in one, two and three dimensions in various shapes. Triangles and quadrilaterals are available in two dimensions while tetrahedrals and hexahedrals (bricks) are provided in three dimensions.

Triangular and tetrahedral elements are geometrically adaptable, especially for complex shapes and they are appropriate for large deformation problems. Although the quadrilaterals and hexahedra elements have a better convergence rate than triangles and tetrahedrals, they will become less accurate when their initial shape is distorted while second-order triangles and tetrahedrals are less sensitive to the initial element shape comparing to other elements. Based on the above fact the second-order triangle has been chosen for modeling soil. Based on these elements behavior, the soil and pipe are modeled as a 2D plane strain model with triangular elements.

2.2 Pipe modeling

In this project, pipe has been discretized with a 6-node quadratic plane strain triangle (CPE6). Pipe is considered as a solid steel pipe with an inner diameter of 0.95 m and thickness of 0.05 m. Since the rigid pipe is stiffer than the surrounding soil, the plastic behavior of pipe is not a matter of interest and the pipe has been modeled with a linear elastic material behavior with Young's modulus of 200 GPa and Poisson's ratio of 0.3. The steel density is assumed to be 7850 kg/m^3.

2.3 Soil modeling

Soil was modeled by a 6-node modified quadratic plane strain triangle (CPE6M). Modified triangular or tetrahedral elements with mid-side nodes use a modified second-

order interpolation and are often called modified elements or modified second-order elements. The most important concern in pipe-soil interaction numerical modeling is the simulation of the soil's stress-strain behavior. In finite element modeling, an elasto-plastic material law with Mohr-Coulomb failure criterion and a non-associated flow rule were considered to describe the behavior of clay and medium dense fine sand.

Mohr-Coulomb plasticity includes a yield function, f, which governs the onset of plastic behavior and the plastic potential function, g, which governs the plastic flow.

$$f = \tau + \sigma \sin\phi - C\cos\phi \quad (2.1)$$

$$g = \tau + \sigma \sin\psi - C\cos\psi \quad (2.2)$$

where τ is the soil shear strength, σ is the soil stress, C is the soil cohesion, φ is the soil friction angle and ψ is the soil dilation angle. Material parameters used in the model are given in Table.1.

2.4 Interfaces

Among varieties of contacts models available in ABAQUS, surface to surface interaction has been used for modeling the interface between soil and pipe. Surface-to-surface contact interactions describe contact between two deformable surfaces or between a deformable surface and a rigid surface.

The interaction between pipe and soil surface consists of two force components. One is perpendicular to the interaction surface, which is the normal behavior, and the other one, tangent to the surface, which is the tangential behavior and consists of sliding between two surfaces and possibly frictional shear stresses. While modeling clay, the pipe-soil

interaction is assumed to be an adhesive friction and no sliding occurs before the shear stress on the surface reaches to its maximum shear stress. This is numerically achieved by assuming a large friction coefficient in Coulomb friction model in the soil-pipe interface. In general, the maximum shear stress τ_{max} along the pipe-soil interface can be assumed to be $1/2C_u$, where C_u is the cohesion of the soil.

In sand the friction coefficient between soil and pipe has a small value. The skin friction angle between soil and steel pipe is about 20-30˚, that will give a friction coefficient between 0.3 - 0.5. In this study sand-steel friction coefficient for the base model has assumed to be about 0.44. (Canadian foundation engineering manual, 1992)

2.5 Modeling steps

Soil is assumed to be finite in the horizontal direction and beneath the pipeline. Therefore, the distances from boundaries are chosen large enough to eliminate the boundary effect and the soil has been modeled by a 50 m x 30 m rectangle. Applied boundary conditions to the soil are pinned support at the bottom with no displacement in the horizontal and vertical direction (u=v=0), and roller support at sides with no movement in the horizontal direction (u=0). The finite element boundary conditions and the oblique pipe displacement angle (α) are shown in Figure 2. The model, shown in Figure 3(a), consists of 1996 triangular shaped elements. The mesh has been refined in areas with stress concentration around the pipeline and soil surface. The mesh density decreases at regions close to the boundaries. In finite element modeling a finer mesh typically results in a more accurate solution, while the computation time will increase. By performing a mesh convergence study, a sufficiently dense mesh with an accurate

solution can be obtained. To determine the most appropriate element number, other models have been created in which the mesh has been refined by adding a denser mesh at the top of the pipeline, using the biased meshing in soil surface. Figure 4 displays the mesh convergence study. The models consist of 763, 1996 and 2453 elements, respectively. Figure 3(b) displays a refined mesh model with 2453 elements as an example. All three models have been subjected to a 0.5D pipe horizontal, vertical and 45° displacements. The difference between the soil maximum resistance between the base model with 1996 elements and the model with 763 elements was about 12% and the difference between the base model and the refined model with 2453 elements was around 1%. As a result, since the base model is less time consuming and is as accurate as the refined mesh, the first mesh has been chosen for this study.

The model has been created in three steps. In the initial step, the pipe and soil initial conditions, like the boundary conditions and the interfaces between soil and pipe, has been defined.

In the next step, a geostatic analysis is first performed to establish the initial stress state in the soil. During this step, the gravity loads are applied and the pipe is allowed to move without rotation. ABAQUS checks for equilibrium during this step using the Mohr-Coulomb soil model to establish a stress field which balances the gravity load and satisfies the boundary condition.

After the geostatic step, the loading step is applied in which the pipe displacement in a given direction will be imposed to the pipe gradually.

2.6 Modeling cohesive material (clay)

To validate the models, buried pipeline in clay soil has been modeled under oblique displacement, α, where α is the inclination angle of pipe movement with respect to the vertical direction. Figure 2 presents the displacement angle, α. The model is a pipe in clay where the clay has undrained shear strength of C_u= 45 kPa, and the pipe burial depth ratio (H/D) is 3.03. (Undrained strength is typically defined by Tresca theory, based on Mohr's circle as: $\sigma_1 - \sigma_3 = 2\,C_u$, Where σ_1 is the major principal stress and σ_3 is the minor principal stress.)

The results have been validated by comparing them to the results in previous studies (Guo, 2005a).

After validating the model, the effect of changes in the soil cohesion on Winkler foundation modulus (K) has been plotted and also the maximum soil resistances in the horizontal and vertical direction have been compared to the ALA soil resistance. The results are discussed in Chapter 3.

2.7 Modeling frictional material (sand)

The next series of modeling is focused on the behavior of buried pipe in frictional material. Based on the equations from ALA discussed above, there are several parameters, such as pipe burial depth and soil friction angle that have high effect on soil behavior. Also, there are some other parameters that have not been considered in ALA equations, such as pipe-soil friction coefficient, soil dilation angle, and initial in-situ stress. In this study the effect of these parameters on the soil-pipe behavior has been studied. These behaviors have been modeled in 48 different cases, by varying

displacement angles (0°, 30°, 45°, 60°, and 90°), different pipe burial depth ratio (1.5, 3, 4.5, and 6), dilation angles (5°, 10°, 20°, and 30°) and also varying friction angles (25°, 30°, and 35°)

Three more cases have been selected to study the effect of friction coefficient on pipe-soil interaction by varying the soil-pipe friction coefficient of 0.25, 0.44 and 0.8.

Also, the effect of initial in-situ stress on the pipe-soil behavior has been studied with initial in-situ stress coefficients of 0.5, 0.75, and 1.

The results are discussed in two parts. In the first part, there will be a discussion about the normalized force-displacement plots and maximum soil resistance in each case. In the second part, there is a discussion on the effect of varying soil parameters on surface heave.

The input parameters for each finite element model are summarized in Table 1.

Table 1. Input parameters in modeled cases

Case	H/D	Soil	E	Density	υ	C_u	φ	ψ	α	Pipe-soil interface friction coeff.	In-situ stress K_0
#			MPa	kg/m^3		kPa	degree	degree	degree		
1	3.03	Clay	18	1600	0.49	45	0	0	90	1	1
2	3.03		18	1600	0.49	45	0	0	60	1	1
3	3.03		18	1600	0.49	45	0	0	45	1	1
4	3.03		18	1600	0.49	45	0	0	30	1	1
5	3.03		18	1600	0.49	45	0	0	0	1	1
6	3.03	Clay	18	1600	0.49	35	0	0	0	1	1
7	3.03		18	1600	0.49	25	0	0	0	1	1
8	3.03		18	1600	0.49	Elastic	-	-	0	1	1
9	3.03	Sand	18	1900	0.33	4	35	10	90	0.44	1
10	3.03		18	1900	0.33	4	35	10	60	0.44	1
11	3.03		18	1900	0.33	4	35	10	45	0.44	1
12	3.03		18	1900	0.33	4	35	10	30	0.44	1
13	3.03		18	1900	0.33	4	35	10	0	0.44	1
14	1.5	Sand	18	1900	0.33	4	35	10	0	0.44	1
15	3.03		18	1900	0.33	4	35	10	0	0.44	1
16	4.5		18	1900	0.33	4	35	10	0	0.44	1
17	6		18	1900	0.33	4	35	10	0	0.44	1
18	3.03	Sand	18	1900	0.33	4	30	10	0	0.44	1
19	3.03		18	1900	0.33	4	35	10	0	0.44	1
20	3.03		18	1900	0.33	4	40	10	0	0.44	1
21	3.03		18	1900	0.33	Elastic	-	-	-	0.44	1

Case	H/D	Soil	E	Density	υ	C_u	φ	ψ	α	Pipe-soil friction coefficient	In-situ stress K_0
#			MPa	kg/m^3		kPa	degree	degree	degree		-
22	3.03	Sand	18	1900	0.33	4	35	0	0	0.44	1
23	3.03		18	1900	0.33	4	35	5	0	0.44	1
24	3.03		18	1900	0.33	4	35	10	0	0.44	1
25	3.03		18	1900	0.33	4	35	20	0	0.44	1
26	3.03		18	1900	0.33	4	35	30	0	0.44	1
27	3.03	Sand	18	1900	0.33	4	35	10	0	0.25	1
28	3.03		18	1900	0.33	4	35	10	0	0.44	1
29	3.03		18	1900	0.33	4	35	10	0	0.8	1
30	3.03	Sand	18	1900	0.33	4	35	20	45	0.44	0.5
31	3.03		18	1900	0.33	4	35	20	45	0.44	0.75
32	3.03		18	1900	0.33	4	35	20	45	0.44	1

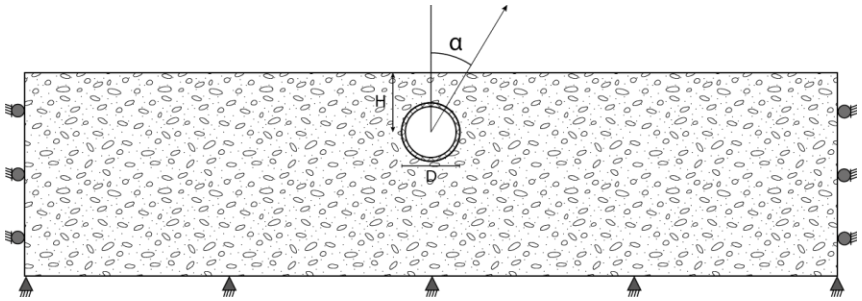

Figure 2 Schematic showing pipe-soil interaction, boundary conditions, and displacement angle

a)

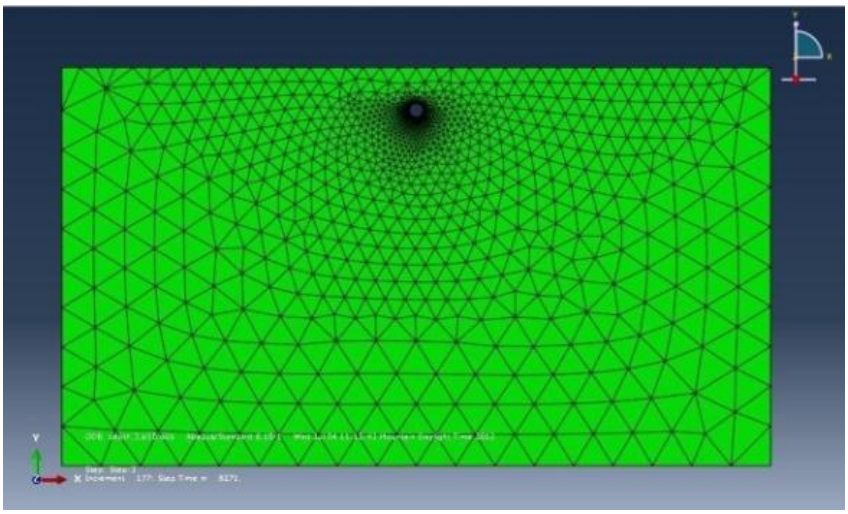

b)

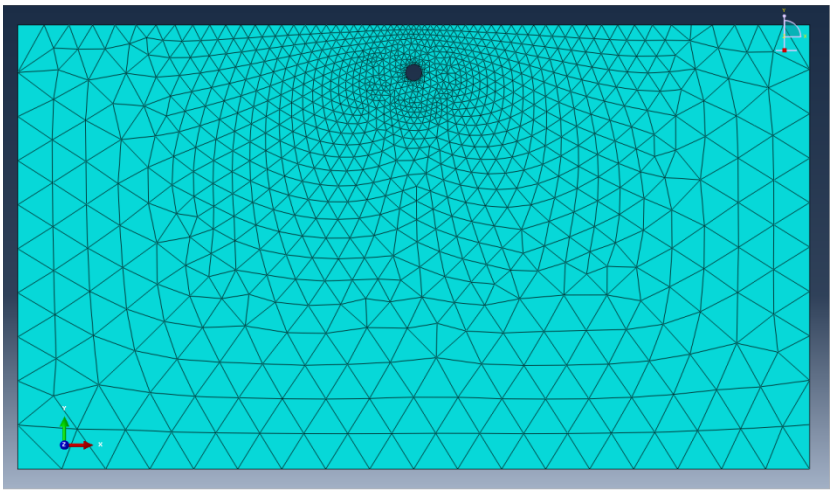

Figure 3 Finite element mesh for pipe-soil interaction: a) Base model with 1996 elements for soil, and b) Refined finite element mesh with 2453 elements for soil

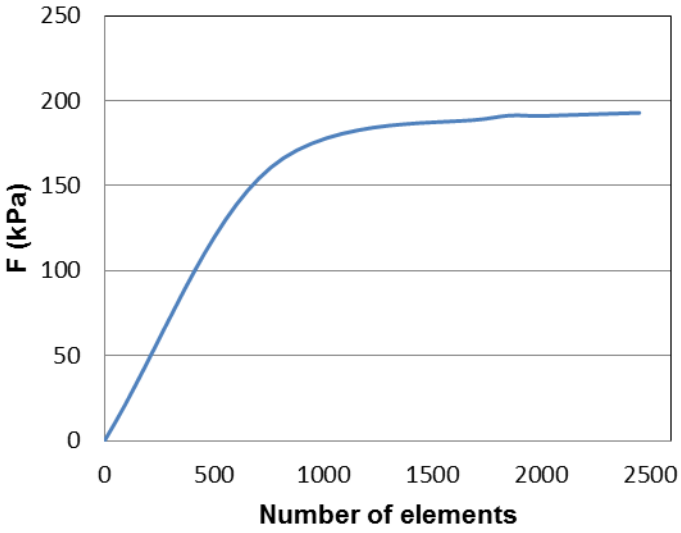

Figure 4 Mesh convergence study

Chapter Three: Results and Discussions

In this chapter the results from finite element modeling has been compared to those predicted by the ALA equations and the proposed failure criterion, using force-displacement curves. In addition, the effect of soil parameters on pipe-soil interaction has been studied using several cases with various soil parameters.

3.1 Behavior in cohesive material (clay)

As discussed before, to validate the model by comparing the results to those from the previous studies (Guo, 2005), the buried pipe in clay has been modeled under varying pipe displacement angles. In this model the burial depth ratio (H/D) is 3, with clay of C_u = 45kPa and the pipe is subjected to different displacement angles (α). Using the finite element results, the total resultant force and its horizontal and vertical components for a given pipe displacement have been calculated and the relevant force-displacement curves have been plotted. Figure 5(a) demonstrates the plot for the normalized total induced force versus the normalized pipe displacement in various displacement directions. Figure 6(a) shows the horizontal component of the induced force versus pipe displacement in the horizontal direction. Figure 7(a) defines the plot for the vertical component of the induced force versus the displacement in the vertical direction. Figures 5(b), 6(b), and 7(b) present the normalized force-displacement plots from Guo (2005), where N_h and N_v are the normalized horizontal and vertical soil resistances for a given displacement (F_h/C_uD and F_v/C_uD), respectively.

General agreement is achieved between the finite element results and those presented by Guo (2005). The main difference between the plots is the slope in the elastic zone of the

model, which may be a result of differences in assumed Young modulus. This is due to lack of information about the presumed Young modulus in Guo's modeling. Furthermore, there is a difference between the consequences of the soil resistances in various pipe displacement between Figures 5(a) and 5(b). This difference rises from a discrepancy between the discussion of the text and Figure 5(b) of Guo's paper. As discussed in his paper, the case with the pipe horizontal displacement (α=90°) should have the highest soil resistance. However, the figure shows a different result, which may be a misprint in the figure.

Based on Figures 5(a), 6(a) and 7(a), the elastic behavior of the pipe is limited to relatively low load levels ($F/C_uD \approx 2.0$). Further loading produces a significantly non-linear deformation. It is clear that by increasing the displacement angle, there will be an increase in the maximum normalized horizontal force component and a decrease in the maximum normalized vertical force component. The horizontal or vertical components of the mobilized soil resistance in the oblique direction are smaller than that when the pipe undergoes purely horizontal or vertical movement (α=90° and α=0°). Figures 8 and 9 display displacement contours for two cases: α=0° and α=45°. In the case of α= 45°, the displacements in the vertical direction are higher than those in the horizontal direction, which is due to the small vertical overburden that results in lower induced forces in the vertical direction.

Figure 10 displays the vertical soil resistance versus the horizontal soil resistance in clay with C_u = 35 kPa when subjected to a normalized δ/D of 0.2. Also, the yield surfaces for δ/D of 0.01, 0.02 and 0.05 have been plotted using F_{h0} of 107.4 kPa, 168.7 kPa, 211.8kPa, and F_{v0} of 98.9kPa, 157.7 kPa, and 187.8 kPa, respectively. The calculated β

for each yield surface would be 1.08, 1.07 and 1.12. Also the failure surface has been plotted using F_{uh0} and F_{uvo} of 220.9 kPa and 191.6 kPa, respectively. Based on the plots, in displacements smaller than $\delta/D=0.02$, there is a linear relation between the soil vertical and horizontal resistance components. Material yields and hardens as it passes through states on successive yield curves. The mobilization of soil resistance can be reflected by the evolution of yield surfaces with pipe displacements and the resistance force will grow toward the maximum resistance force.

Table 2 gives the maximum soil resistance for different pipe displacement angles. Based on the results, by increasing pipe displacement angles, the maximum soil resistance will increase, and consequently the maximum soil resistance in the horizontal direction is 15% higher than the maximum soil resistance in the vertical direction.

- **Cohesion**:

  In natural soils, cohesion results from electrostatic bonds between clay particles and the strength of a soil is a combination of the cohesive and frictional contributions. Thus by increasing soil cohesion, the soil maximum resistance will increase.

  To study the effect of soil cohesion on the pipe-soil interaction, three cases has been model with different cohesion values of C_u=25, 35 and 45 kPa for a pipe burial depth ratio (H/D) of 3.03. The force-displacement results for these cases have been plotted in Figure 11. Also, an elastic case has been modeled to compare the elastic model to the elasto-plastic model. In all these four cases, the pipe has been subjected to an upward displacement (α=0).

Since the main objective of this section is to investigate the effect of soil cohesion on the maximum soil resistance, the results in Figure 11 are displayed as total force versus normalized displacement. Based on the results, soil with a higher cohesion, shows a higher maximum soil resistance. The results indicate that by increasing soil cohesion from 25 kPa to 35 kPa and then from 35 kPa to 45 kPa, the maximum soil resistance will increase 26% and 21%, respectively. Tables 3 and 4 compare the results from finite element modeling with those from ALA guideline. In Table 3, the ALA horizontal and vertical upward soil bearing capacity factor, N_{ch} and N_{cv} has been compared to the horizontal and the vertical upward capacity factor, F_h/C_uD and F_v/C_uD from the finite element analysis. According to the ALA (2001), N_{ch} and N_{cv} are independent on soil cohesions. Varying the soil cohesion will not affect their values, while the horizontal and vertical upward bearing capacity factors from finite element modeling are highly affected by the cohesion factor. Although they have been normalized by the cohesion factor, the bearing capacity factor will decrease with increasing soil cohesion. For the clay with cohesion of 25 kPa the ALA upward bearing capacity factor (N_{cv}) and the upward bearing capacity factor calculated from finite element modeling (F_v/C_uD), are both 6.37. For clay with a larger cohesion, ALA predicts a lower upward capacity factor than finite element modeling. Since the ALA has considered the soil cohesion effect on the soil maximum resistance (P_u), and not the bearing capacity factor (N_{cv}), Table 4 compares the horizontal and upward maximum resistances from ALA (2001) and finite element modeling.

With respect to Table 4, in both ALA and finite element modeling with increase in soil cohesion, the maximum horizontal and vertical soil resistance (F_v and F_h) will increase,

which is a reasonable behavior based on the equations (1.2) and (1.5). The ALA (2001) predicts the maximum vertical resistance (Q_u) for soil with cohesion 25, 35 and 45 kPa about 1%, 9% and 15% higher than the finite element modeling. On the other hand, for the maximum horizontal resistance (P_u), the ALA (2001) gives a more conservative value. For clay with 25 and 35 kPa cohesive strength the ALA horizontal maximum resistances are 7% and 4 % lower than those from the finite element modeling.

Figure 11 compares the results from the elastic analysis and the elasto-plastic analysis. All cases will follow the linear elastic behavior in pipe small displacement and the induced force is proportional to the displacement. By increasing pipe displacement, in the elasto-plastic cases the plastic deformation will be developed according to the yield and plastic potential function, while in the elastic case the elastic deformation will grow linearly. In the elastic model the soil resistance is overestimated, as a result of not considering material plastic deformation.

3.2. Behavior in frictional material (sand)

To study the frictional material behavior, several pipe-sand cases have been modeled with ABAQUS using modeling parameters shown in Table 1. The base case is a sand model with a friction angle of 35° and a dilation angle of 10°. Also, to avoid the model convergence in the geostatic step, a small cohesion of 4 kPa has been assigned to the sand model. Sand parameters have been varied to analyze the effect of each parameter on the pipe-sand interaction behavior.

3.2.1. Effect of pipe burial depth

To design a buried pipeline, the minimum depth of soil cover that can provide sufficient uplift resistance is a matter of concern. Since the capability of the soil to resist the pipeline movement can affect the occurrence of upheaval buckling, pipeline burial depth can highly affect the construction costs and it is important to find the safe and shallow burial depth for the pipeline.

To find the most effective pipe burial depth, different values of burial depth, H, have been modeled with a constant pipe diameter of 0.95 m. The modeled burial depth ratios are: H/D=1.5, 3, 4.5 and 6. To study the effect of burial depth on the soil maximum uplift resistance, the results are plotted as a normalized force-displacement graph for each case, in Figure 12. The soil normalized maximum resistance per unit length of pipe is highly affected by the pipe burial depth ratio (H/D) and by increasing the burial depth ratio, the soil normalized maximum resistance increases. As observed in the curves for the shallower pipelines the normalized maximum resistance develops at a small displacement while for pipelines with a higher H/D, a larger pipe displacement is required to mobilize the maximum soil resistance.

Figures 13 and 14 compare the surface heave using displacement contours for two cases with H/D of 1.5 and 6 for the same amount of pipe displacement. Both cases have the same soil parameters (E, υ, and φ,...) and only the pipe burial depth differs. Based on these figures it is clear that the pipe with a lower H/D has a higher surface heave. For the pipe with H/D of 6, the surface heave is less than half of the surface heave for the case with H/D of 1.5. The surface heave will be discussed on section 3.3.

Furthermore, ABAQUS calculates the plastic strain by decomposing the total strain values into the elastic and plastic strain components. The plastic strain is obtained by subtracting the elastic strain from the value of total strain:

$$\varepsilon^{pl} = \varepsilon^{t} - \varepsilon^{el} = \varepsilon^{t} - \sigma/E \qquad (3.1)$$

Figures 15 and 16 compare the plastic strain contours for pipelines with burial depth ratios of 1.5 and 6, respectively. In the case with burial depth ratio of 6, the plastic zone has not reached to the surface while for the case with depth ratio of 1.5 there is a small plastic strain beneath the soil surface which will result in an earlier failure in smaller burial depth.

3.2.2. Effect of pipe displacement angle

To study the effect of pipe displacement angle on the pipe-soil interaction, the pipe-sand interaction has been modeled with different displacement angles, α. In all cases, the burial depth ratio (H/D) is 3.03 with a sand friction angle of φ=35° and a dilation angle of ψ=10°. Pipe displaces along different angles α of 0°, 30°, 45°, 60° and 90°, with respect to the vertical direction.

Figure 17 compares the normalized force-displacement curves for different pipe displacement angles when the pipe is subjected to a normalized displacement of δ/D=0.4. Similar to the behavior in clay, the elastic response is limited to a very small pipe displacement, and the plastic region will grow with a larger displacement. Also, by increasing the displacement angle, the maximum soil resistance will increase. The normalized horizontal and vertical force components versus the normalized horizontal and vertical pipe displacement components have been plotted in Figures 18 and 19,

respectively. An increase in pipe displacement angle, α, will result in an increase in the normalized maximum horizontal resistance, while by increasing the displacement angle, the normalized maximum vertical soil resistance will decrease. Also, with an increase of α, a smaller displacement is required to mobilize the maximum soil horizontal resistance, while the maximum soil vertical resistance will develop at a larger displacement.

Table 5 gives the maximum resistance force for different pipe displacement angles. Based on the results in Table 5 and Figure 17, by increasing the pipe displacement angle from the vertical direction ($\alpha=0^{o}$) to the horizontal direction ($\alpha=90^{o}$), the soil maximum resistance will increase.

Figure 20 displays the vertical soil resistance component versus the horizontal soil resistance component in sand when the pipe is subjected to a displacement of δ/D=0.3. Also, the yield surfaces for δ/D of 0.01, 0.02, and 0.05 have been plotted using F_{h0} of 89.5 kPa, 161.2 kPa, 292.3.8kPa, and F_{v0} of 75.7 kPa, 104.7 kPa, and 149.1 kPa, respectively. The calculated β for each yield surface would be 1.18, 1.54 and 1.96. Also the failure surface has been plotted using F_{uh0} and F_{uvo} of 313.6 kPa and 156 kPa, respectively. In small pipe displacements less than δ/D=0.01, there is a linear relation between the soil vertical and horizontal resistance components, while by increasing pipe displacement, the material yields and hardens as it passes through the states on the successive yield surfaces and the soil resistance will grow toward the maximum resistance force. There is a general agreement between the proposed yield surfaces of equation (1.13) and the results from the finite element modeling. While comparing the FEM results with the proposed failure envelope of equation (1.10), the induced forces

plots do not reach to the proposed failure envelope and the proposed failure envelope overestimates the induced forces at failure.

Furthermore, based on Figure 20, by increasing the pipe displacement, the rate of increase in the soil maximum resistance in the vertical direction is smaller than that in the horizontal direction.

3.2.3. Effect of sand friction angle

Based on equations (1.3) and (1.4), the coefficients a, b, c, d and e are highly affected by the friction angle that can emphasize the high effect of friction angle on the maximum soil horizontal resistance predicted by ALA (2001). Also, in ALA (2001) equations the friction angle has a direct relationship with the maximum vertical resistance of soil. To study these relations in sand, several cases have been modeled using sands with friction angles of 30°, 35° and 40° and a constant dilation angle of 10°. In all these four cases the pipe burial depth ratio (H/D) is 3.03 and the pipeline has been subjected to a vertical displacement (α=0°).

Figure 21 displays the normalized force-displacement plot for each case. Based on the plots, an increase in the friction angle will result in an increase in the maximum soil resistance and increase in the mobilized δ/D.

Based on Mohr-Coulomb yield function, the plastic failure develops if the shear stress τ_n on a plane exceeds a constant fraction of the normal stress σ_n:

$$|\tau_n| = \tan\phi\, \sigma_n + C \quad (3.2)$$

where tan(ϕ) is the coefficient of friction and C is soil cohesion.

As a result of increase in internal friction angle (i.e. increase in the strength of the material) the shear strength of the soil will increase and directly affects the peak value in the normalized resistance force. In Figure 21, by increasing φ from 30° to 40°, an increase of more than 12% in the soil maximum resistance is revealed.

Also, by increasing the soil friction angle from 35° to 40°, the displacement in which the soil will reach to its maximum resistance will increase about 18%.

The finite element modeling results also show the significant effect of the friction angle on the soil plastic deformation. As discussed in equation (3.1), ABAQUS calculates the plastic strain of the material as a scalar variable to represent material's plastic deformation. As shown in Table 6, there would be less plastic deformation for the higher values of internal friction angle. This phenomenon might seem obvious since the plastic deformation is less for stronger material at a given stress level. This can be further clarified using plasticity theory.

Considering a non-associated flow rule, the plastic deformation can be derived as:

$$\dot{\varepsilon}^p = \dot{\lambda}\frac{\partial g}{\partial \sigma} \qquad (3.3)$$

with g being the plastic potential function. Considering the Drucker's consistency postulate, $\dot{\lambda}$, can be found as:

$$\dot{\lambda} = \frac{\frac{\partial f}{\partial \sigma}.C^e.\dot{\varepsilon}}{\left(\frac{\partial f}{\partial \sigma}.C^e.\frac{\partial g}{\partial \sigma}\right) + R}$$

$$R = -\frac{\partial f}{\partial \varepsilon^p}.\frac{\partial g}{\partial \sigma} \qquad (3.4),$$

where:

f: yield function

g: plastic potential function

$\dot{\lambda}$: plastic multiplier

C^e: total Stress increment tensor

$\dot{\varepsilon}$: total stress increment tensor

If we consider the normal forces, for example, the term $\frac{\partial f}{\partial \sigma}$ is equal to the mobilized friction angle which is a direct function of the ultimate internal friction angle at failure. If we assume that $\frac{\partial f}{\partial \sigma_n} = \tan \phi^m$, then the change in λ due to the change in mobilized friction angle can be calculated as follows:

$$\frac{\partial \dot{\lambda}}{\partial \tan \phi^m} = \frac{R \tan \phi^m}{\left[\left(\frac{\partial f}{\partial \sigma_n}.C^e.\frac{\partial g}{\partial \sigma_n}\right)+R\right]^2} \quad (3.5)$$

Since R is a negative parameter in the equation above, we can imply that $\dot{\lambda}$ decreases with increase in the mobilized friction angle; hence the plastic deformation decreases as the friction angle increases.

3.2.4. Effect of sand dilation angle

Based on Taylor (1948) stress-dilatancy rule:

$$\frac{\tau_{peak}}{\sigma'} = \tan \phi'_m = \mu + \left(\frac{dy}{dx}\right) \quad (3.6)$$

The peak shear stress ratio ($\frac{\tau_{peak}}{\sigma'}$) consists of components of interlocking (dy/dx), which shows rate of dilation, and sliding friction between grains, μ. Therefore, the peak shear stress ratio directly depends on the dilation angle.

In frictional soils the angle of dilation controls the amount of plastic strain developed during shearing and it is assumed to be constant during plastic yielding.

$$d = -\frac{d\dot{\varepsilon}_V}{d\Upsilon} = -\frac{\dot{\varepsilon}_1+\dot{\varepsilon}_3}{\dot{\varepsilon}_1-\dot{\varepsilon}_3} = \sin\Psi \qquad (3.7)$$

It is obvious that for a dilation angle greater than zero the plastic volumetric strain rate will be negative and therefore lead to dilation.

Besides, as discussed before, in the non-associated flow rule the plastic strain rates are written as:

$$\dot{\varepsilon}^p = \dot{\lambda}\frac{\partial g}{\partial \sigma} \quad (3.8)$$

where $\dot{\varepsilon}^p$ is the plastic strain-rate, λ is a non-negative multiplier, σ is the Cauchy stress tensor and g is the plastic potential function which depends on the stress and on the instantaneous dilation angle ψ.

The effect of dilation angle has been studied using the base case, sand with friction angle of 35° and cohesion of 4 kPa with pipe burial depth ratio of 3.03, and varying dilation angles of ψ= 0°, 5°, 10°, 20°, and 30°.

Based on the plotted results on Figure 22, by increasing the dilation angle, the soil stiffness does not change significantly and the maximum resistance achieved will be

around the same displacement as it happens in other cases, which is about 0.05D. While by increasing the dilation angle the maximum soil resistance will increase considerably.

3.2.5. Effect of pipe-soil friction coefficients

The effect of pipe and soil friction coefficient on pipe-soil interaction has been studied with varying friction coefficients of 0.25, 0.44, and 0.8. In all cases the pipe burial depth ratio (H/D) is 3.03, the friction angle is $\varphi = 35^{\circ}$ and the dilation angle is $\Psi=10^{\circ}$. The pipe is subjected to a vertical displacement, $\alpha=0^{\circ}$.

Figure 23 indicates that the decrease in the soil-pipe interface friction does not significantly affect the soil maximum resistance. Among these three cases, the case with pipe-soil friction coefficient of 0.44 has the highest soil maximum resistance compared to the other cases. The maximum soil resistance for this case is about 1% higher than the other coefficient that is negligible.

Cases with a friction coefficient smaller than 0.2, will fail at the first step of loading while subjecting to the pipe displacement.

3.2.6. Effect of in situ stress coefficient

The in situ stresses represent an important initial condition for geotechnical analysis. It controls the distribution of stresses under soil surface. Typically, the horizontal stress is computed from the vertical stress using the coefficient of earth pressure at rest, K_o, which depends on micro-structure of the soil, geometry of the soil, stress history and relative density of soil.

In this project, the effect of coefficient of earth pressure at-rest on the maximum soil resistance has been verified by modeling three sand samples with the cohesion of 4 kPa,

the dilation angle of 20° and H/D= 3.03, using different K_o of 0.5, 0.75, and 1 and pipe displacement of α=45°.

Based on the results in Figure 24 and also Table 7, by increasing the coefficient of earth pressure at-rest from 0.5 to 1, the soil maximum resistance increases about 1.5%. Although the coefficient of earth pressure at-rest has a small effect on the soil maximum resistance, it has a higher effect on the soil maximum horizontal resistance. This is due to the dependency of the stress distribution to the coefficient of earth pressure at-rest

Also, in Table 8 the surface heave results display that by increasing the coefficient of earth pressure at-rest from 0.5 to 1, the surface heave will increase about 0.57%.

3.2.7. Linear elastic case versus elasto-plastic case.

Based on theory of plasticity, the strains and strain rates are decomposed into an elastic part and a plastic part, where:

$\underline{\varepsilon} = \underline{\varepsilon}^e + \underline{\varepsilon}^p$ and $\underline{\acute{\varepsilon}} = \underline{\acute{\varepsilon}}^e + \underline{\acute{\varepsilon}}^p$

Figure 25 compares the force-displacement curve for an elastic case and a plastic case with friction angle of 35°, dilation angle of 10° and soil cohesion of 4 kPa. The pipe burial depth ratio for both cases is H/D=3.03. The models behave the same up to the yield point and then the plastic case behaves based on the assigned failure envelope. Based on the plot, the elastic case overestimates the soil maximum resistance.

It is obvious that the linear elastic model is usually inappropriate to model the highly non-linear behavior of soil, unless the modeling is for very small elastic displacements.

3.2.8. Superimposition of effects

Different cases with varying soil parameters were studied to define the effect of each parameter on the soil maximum resistance and the surface heave. The effect of each parameter on the surface heave will be discussed on section 3.3. The maximum soil resistance from the finite element analysis for some parameters has been summarized in Tables 9 to 13. Based on Table 9 with the pipe displacement in any direction, by increasing the dilation angle, the soil maximum resistance will increase. Also, as the pipe displacement goes from the vertical direction to the horizontal, soil will have a higher total maximum resistance. In the vertical pipe displacement, by increasing soil dilation angle from 0° to 20° the soil maximum resistance will increase 26%, while in the horizontal pipe displacement, it will increase 33%.

In Table 10, the effect of the friction angle and pipe burial depth ratio on the soil maximum resistance has been compared. An increase in the friction angle has a higher effect on the maximum resistance of soil in deeper pipelines comparing to shallow pipelines.

Table 11 compares the vertical and horizontal soil maximum resistance components for different pipe displacement angles, α. Table 12 compares the effect of the pipe burial ratio (H/D) on the soil maximum resistance, while the pipe is subjected to different displacement angles. As discussed before by increasing the pipe burial ratio from 1.03 to 3.03, the soil maximum resistance will increase 230%, 250% and 300% for the horizontal, 45^{o} and the vertical pipe displacement, respectively.

Based on the previous discussions and Table 13 for a pipe-soil friction coefficient of 0.25, soil fails with very small displacement, and by increasing friction in pipe-soil interface, pipe-soil strength increases significantly up to a friction coefficient of 0.35 and then it will increase with a very low rate.

3.2.9. Yield surface and Failure envelope

Based on the results presented on Figures 26 to 28, the proposed failure envelope has been plotted for pipe in frictional soil. Figure 26 compares Guo's proposed failure envelope of equation (1.10) in pipes with different burial depth ratios of H/D for soil friction angle of 35° and dilation angle of Ψ=10 °. There is a general agreement between the results from the proposed failure envelope and finite element simulation. By increasing pipe burial depth, the soil maximum horizontal and vertical resistance will increase.

Figure 27 displays normalized values of F_h and F_v with F_{h0} and F_{v0}, and compares them to equation (1.10).

Also, using the results from the sand case with the pipe burial depth ratio of H/D=3.03, φ=35°, and Ψ=10°, the yield envelope has been constructed to compare the results from finite element modeling and the proposed yield surface by Guo (2005). Figure 28 studies soil behavior with varying pipe displacement magnitude, δ/D during soil hardening, using both Guo's proposed model and finite element analysis. General agreements are achieved between the results obtained from the proposed model and the finite element simulation.

Furthermore, Table 14 compares the soil bearing capacity factors predicted by ALA (2001) guideline to the results from finite element modeling. The soil bearing capacity factors and soil maximum resistance have been compared for the parameters that affect the soil maximum resistance most.

In models with different friction angles, by increasing soil friction angle, the soil bearing capacity factor will increase in both ALA and FEM. For sand with friction angles of 30° and 35°, ALA guideline gives soil bearing capacity factors lower than the finite element model which will be more conservative, while for a soil with a friction angle of 45°, the maximum bearing capacity factor predicted from the ALA is 2% higher than those calculated by the finite element model.

Since the dilation angle is not considered in the maximum soil resistance calculations in ALA (2001) guideline, for the models with dilation angles of 0°, 5°, 10°, 20° and 30°, the predicted maximum bearing capacity factor from ALA is a constant value, while the FEM model shows that an increase in the dilation angle will result in an increase in the soil maximum bearing capacity factor. The ALA overestimates the maximum soil resistance only for dilation angles of 0° and 5°, while by increasing the dilation angle to 30°, the maximum soil resistance predicted from ALA is about 12% lower than the FEM results, consequently giving conservative results.

In cases with different pipe burial depth ratio, by increasing pipe burial depth the soil maximum resistance will increase in both ALA and finite element method. The ALA guideline overestimates the maximum soil resistance in the model with pipe burial depth

ratio of 1.5, while for the higher depth ratios the soil maximum resistances predicted by ALA are around 4% to 45% smaller than the FEM results.

In overall, with respect to the results in Tables 14 the results predicted from the ALA guideline are more conservatives in most cases, except in the cases with shallow pipelines, soil with a high friction angle, or soil with a zero dilation angle. By applying a coefficient of 0.8 to the ALA guidelines will result in predicting a conservative soil maximum resistance.

3.3 Surface heave

The induced loads to the pipeline may cause displacement in the pipeline which can result in ground movement, soil settlement or surface heave. Ground movements are a major concern when the pipeline is displaced in close proximity to other utilities. The magnitude of ground movement needs to be estimated to manage the risk of damage to other infrastructure. Empirical guidelines are often used to prevent disturbance to adjacent infrastructure during pipeline displacement.

In this project, the finite element analysis has been used to examine the surface heave caused by pipeline displacement in frictional soil with a friction angle of 35° and varying dilation angles of 10°, 20°, and 40°.

The effect of dilation angle and loading angle on the surface heave was plotted in Figures 29, 29, and 30 for the vertical, 45° and the horizontal pipe displacement, respectively. The results have been normalized by plotting the surface heave over the pipe displacement (u/δ), versus the pipe displacement over the pipe diameter (δ/D). Based on the plots the smallest surface heave happens for the horizontal pipe displacement. Comparing the vertical and the horizontal pipe displacements (Figures 29 and 31), when the pipe is subjected to a horizontal displacement, the resultant surface heave will be about 25% of the surface heave that a vertical pipe displacement can cause.

Comparing among various pipe burial depths in the Figures 29, 30, and 31, for the case with a pipe burial ratio of 1.5, an increase in the dilation angle has the highest effect on the surface heave. By increasing the pipe burial depth ratio from 1.5 to 6, the effect of changes in the dilation angle on the surface heave will be less. Also, the soil model with a

dilation angle of 40° has a higher surface heave comparing to the soil with lower dilation angles.

Furthermore, to examine the surface horizontal displacement, the horizontal displacement for the point with the maximum surface heave has been plotted versus pipe burial depth ratio. The horizontal displacement has been normalized with pipe diameter. The results are shown in Figures 32 and 33 for pipe displacement in the 45° direction and the horizontal direction. In these figures the soil horizontal displacement is symbolized by "u". Based on these figures, the dilation angle does not affect the surface horizontal displacement significantly. While by increasing pipe burial depth, the surface horizontal displacement will decrease.

In the pipe horizontal displacement (α=0°), by increasing the soil dilation angle, the surface horizontal displacement would remain almost the same. In Figure 32 the displacement for the pipe burial ratio of 1.5 has a smaller amount as compared to the displacement for the pipe burial ratio of 3. That is because of the earlier failure in the shallow buried pipe models. Since the soil fails sooner in shallower pipes comparing to the deeper pipes, in pipe burial ratio of 1.5 the pipe cannot be modeled under higher pipe displacement.

Displacement angle	0°	30°	45°	60°	90°
$F_{maximum}$ (kPa)	191	194	200	208	220
δ/D	0.077	0.111	0.075	0.095	0.081

Table 2. Effect of pipe displacement angle (α) on clay maximum resistance (H/D=3.03, C_u=35 kPa)

Soil cohesion (kPa)	N_{cv} (ALA)	F_v/C_uD (FEM)	N_{ch} (ALA)	F_h/C_uD (FEM)
25	6.37	6.37	6.37	7.26
35	6.37	5.76	6.37	6.65
45	6.37	5.38	6.37	6.36

Table 3. Comparison of vertical and horizontal bearing capacity factors estimated from ALA (2001) and finite element modeling (C_u=45 kPa, H/D=3.03, α=0)

Soil cohesion (kPa)	Q_u (kPa) (ALA)	F_v (kPa) (FEM)	P_u (kPa) (ALA)	F_h (kPa) (FEM)
25	151.2	151.3	151.4	172.4
35	212.1	191.5	212.0	221.1
45	272.7	230.3	272.5	271.8

Table 4.Comparison of vertical and horizontal soil resistance estimated from ALA(2001) and finite element modeling (C_u=45 kPa, H/D=3.03, α=0)

Pipe displacement (α)	0°	30°	45°	60°	90°
$F_{maximum}$ (kPa)	156	182	213	263	313
δ/D	0.10	0.14	0.13	0.16	0.11

Table 5. Effect of pipe displacement angle (α) on sand maximum resistance (H/D=3.03, ϕ=35° and Ψ=10°)

φ	30°	35°	40°
Plastic strain (%)	1.91	1.88	1.86

Table 6. Effect of friction angle on plastic deformation (H/D=3.03, Ψ=10°and α=0°)

Soil	K_o=0.5	K_o=0.75	K_o=1
Maximum Soil Resistance (kPa)	236.8	239.5	240.5
Maximum Horizontal Soil Resistance (kPa)	218.6	222.2	223.2
Maximum vertical Soil Resistance (kPa)	107.8	108.2	108.9

Table 7.Maximum sand resistance for varying K_o (H/D=3.03, ϕ=35°, Ψ=10°, α=45°)

	K_o=0.5	K_o=0.75	K_o=1
Surface Displacement	3.41E-01	3.42E-01	3.43E-01

Table 8. Sand surface Heave for varying K_o (H/D=3.03, ϕ=35°, Ψ=10°, α=45°)

Displacement angle, α^o	$F_{maximum}$ (kPa)			
	$\psi=0^o$	$\psi=5^o$	$\psi=10^o$	$\psi=20^o$
0	128.3	132.2	157.3	162.8
30	159.8	174.6	182.3	196.3
45	187.4	208.9	212.5	236.7
60	206.0	233.0	261.1	293.3
90	248.5	304.9	312.9	331.3

Table 9. Effect of dilation angle and pipe displacement angle on maximum resistance in sand for H/D=3.03 and $\phi=35^o$

H/D	$F_{maximum}$ (kPa)		
	$\Phi=30°$	$\Phi=35°$	$\Phi=40°$
1.5	51.6	54.3	56.9
3	146.2	156.0	164.1
6	483.7	543.7	595.1

Table 10. Effect of friction angle and pipe burial depth on maximum resistance in sand for pipe vertical displacement ($\alpha=0°$) and $\Psi=10°$

Displacement angle, α^o	$F_{maximum}$ (kPa)		
	F	F_h	F_v
0	156	0	156
30	182.4	128.5	133.1
45	213.0	190.1	106.5
60	263.3	259.5	81.2
90	313.6	313.6	0

Table 11. Effect of different displacement angle on horizontal and vertical maximum resistance components in sand for H/D=3.03, $\phi=35^o$ and $\Psi=10^o$

H/D	$F_{maximum}$ (kPa)		
	$\alpha=0^o$	$\alpha=45^o$	$\alpha=90^o$
3.03	128.3	187.4	248.5
1.03	31.6	57.5	74.5

Table 12. Effect of different displacement angles and pipe burial ratio on maximum resistance in sand for $\phi=35^o$ and $\psi=0^o$

α^o	$F_{maximum}$ (kPa)		
	Friction Coeff.=0.25	Friction Coeff.=0.44	Friction Coeff.=1
0	155.8	155.8	155.8
45	212.5	212.5	212.5
90	312.6	312.7	312.6

Table 13. Effect of pipe-soil friction coefficient on maximum resistance in sand for H/D=3.03, ϕ=35° and ψ=10°

φ °	ψ °	H/D	N_{qv} (ALA)	$F_v/\gamma HD$ (FEM)	Q_u (kPa) (ALA)	F_v (kPa) (FEM)
°	°				kPa	kPa
30	10	3	2.	2.8	131.5	146.2
35	10	3	2.4	3.0	149.4	156.0
40	10	3	2.7	3.1	167.3	164.1
35	0	3	2.4	2.8	149.4	146.6
35	5	3	2.4	2.9	149.4	150.7
35	10	3	2.4	3.0	149.4	156.0
35	20	3	2.4	3.1	149.4	162.9
35	30	3	2.4	3.2	149.4	170.2
35	10	1.5	2.4	2.0	61.9	54.2
35	10	3	2.4	2.9	149.4	155.8
35	10	4.5	2.4	3.6	221.9	289.6
35	10	6	2.4	5.1	295.9	543.7

Table 14.Comparision between bearing capacity factors and soil maximum resistances estimated from ALA (2001) and finite element modeling in sand

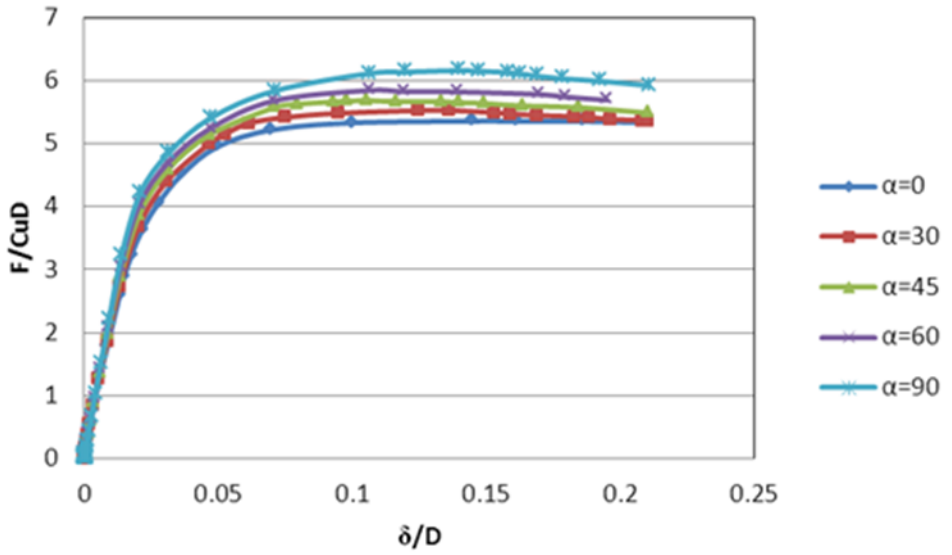

a)

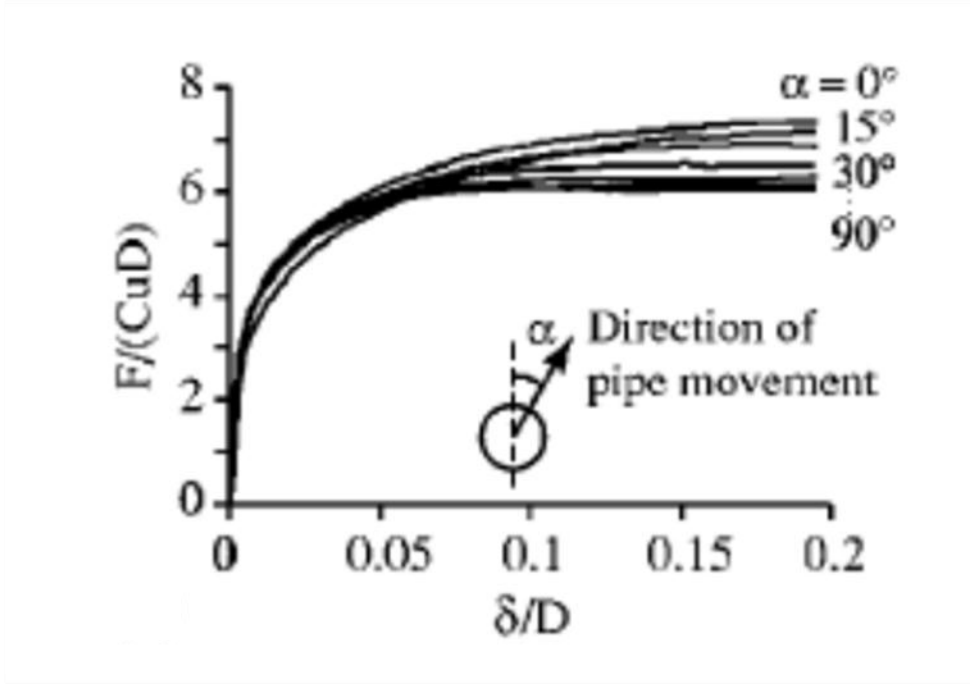

b)

Figure 5 Dependency of force-displacement responses on pipe displacement angle for H/D=3.03, Cu=45 kPa, for total soil resistance, a) FEM results, and b) Guo (2005)

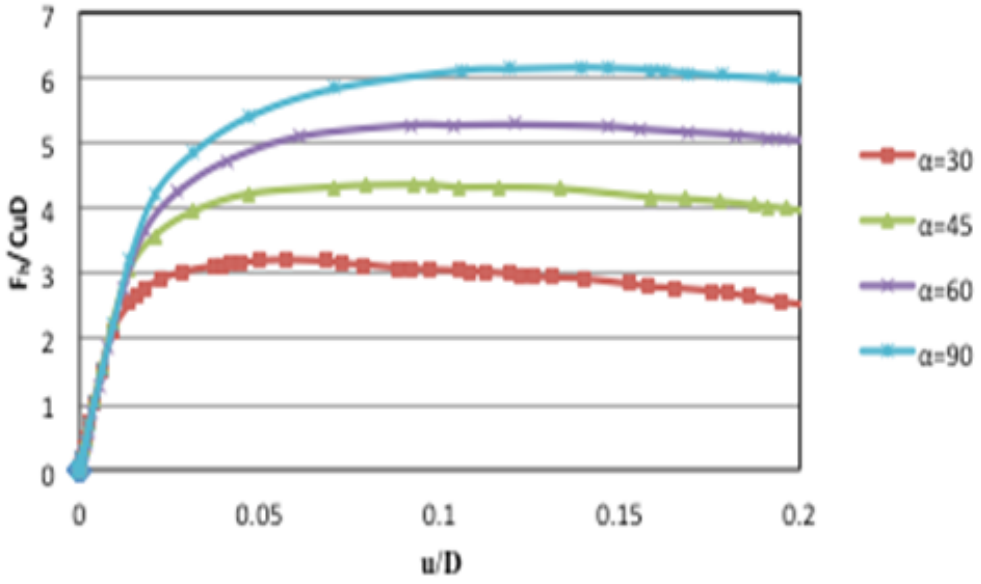

a)

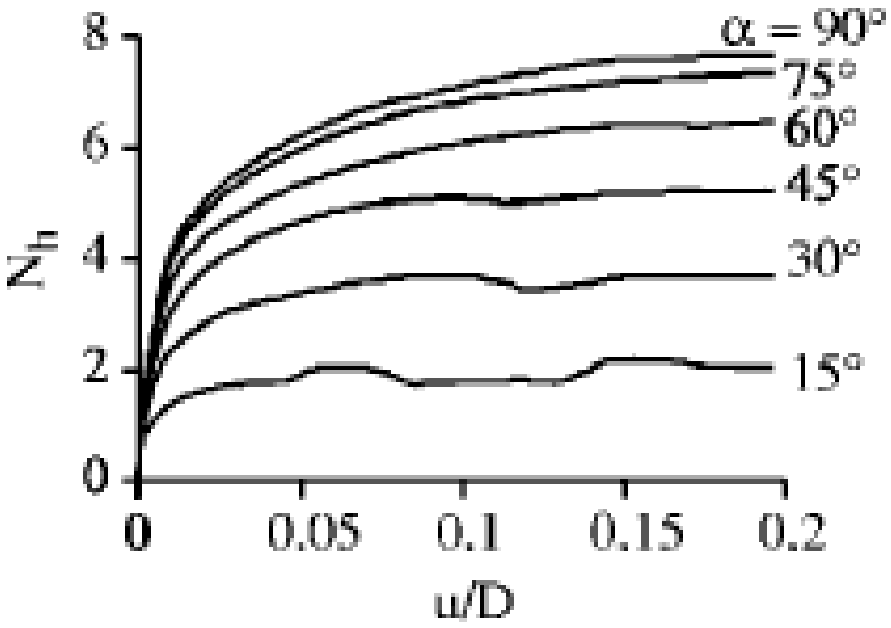

b)

Figure 6 Dependency of force-displacement responses on pipe displacement angle for H/D=3.03, Cu=45 kPa, for the horizontal component of soil resistance a) FEM results, and b) Guo (2005)

a)

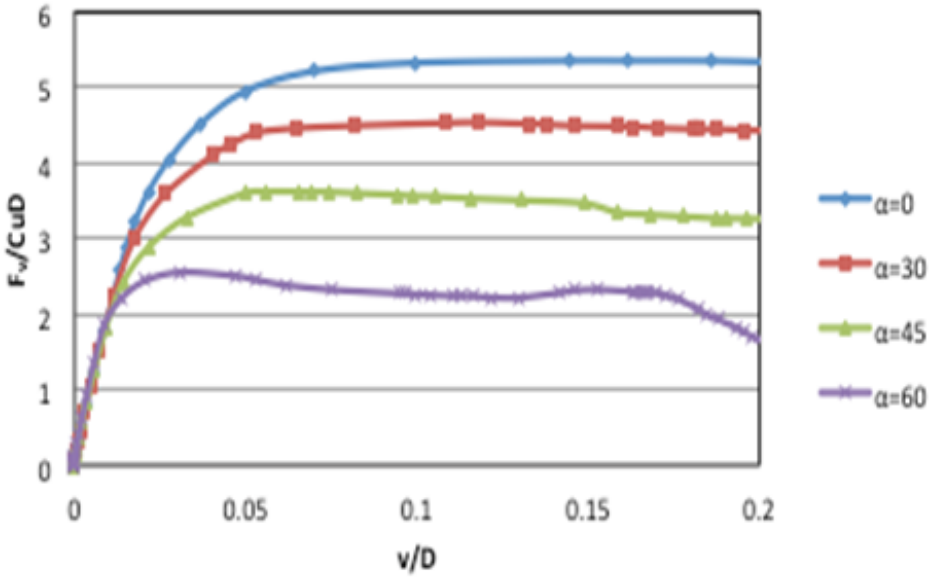

b)

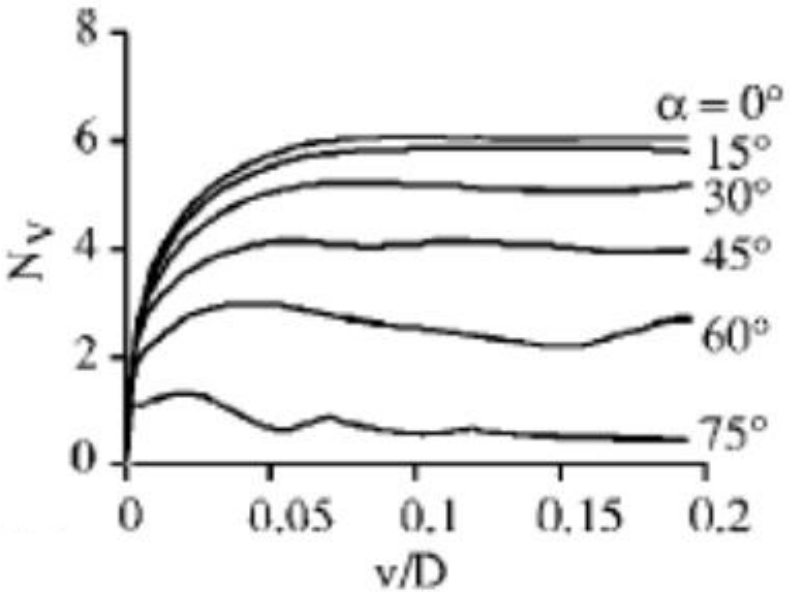

Figure 7 Dependency of force-displacement responses on pipe displacement angle for H/D=3.03, Cu=45 kPa, for the vertical component of soil resistance a) FEM results, and b) Guo (2005)

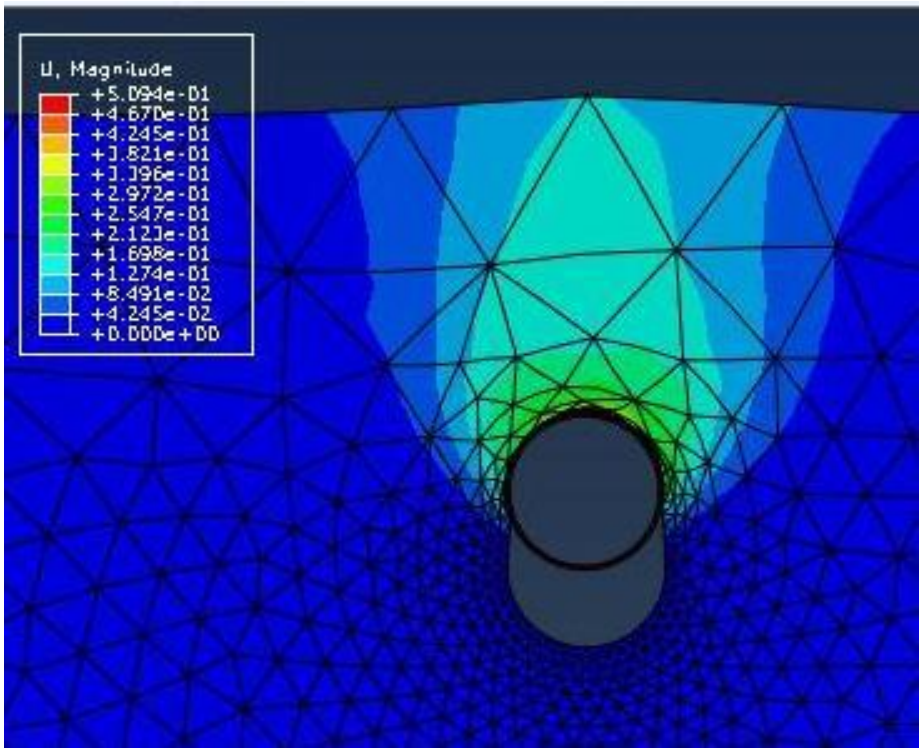

Figure 8. Deformed finite element mesh as a result of pipe vertical displacement of $\delta/D=0.3$, $\alpha=0^{o}$, (C_u=45 kPa, H/D=3.03), Displacement contours (m)

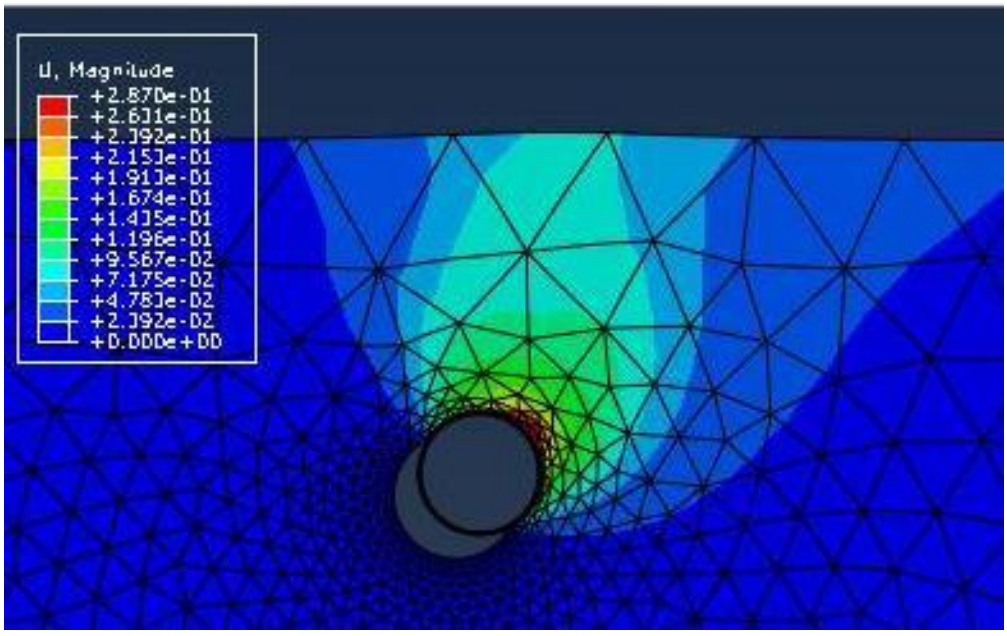

Figure 9. Deformed finite element mesh as a result of pipe oblique displacement of $\delta/D=0.3$, $\alpha=45^{o}$, (C_u=45 kPa, H/D=3.03), Displacement contours (m)

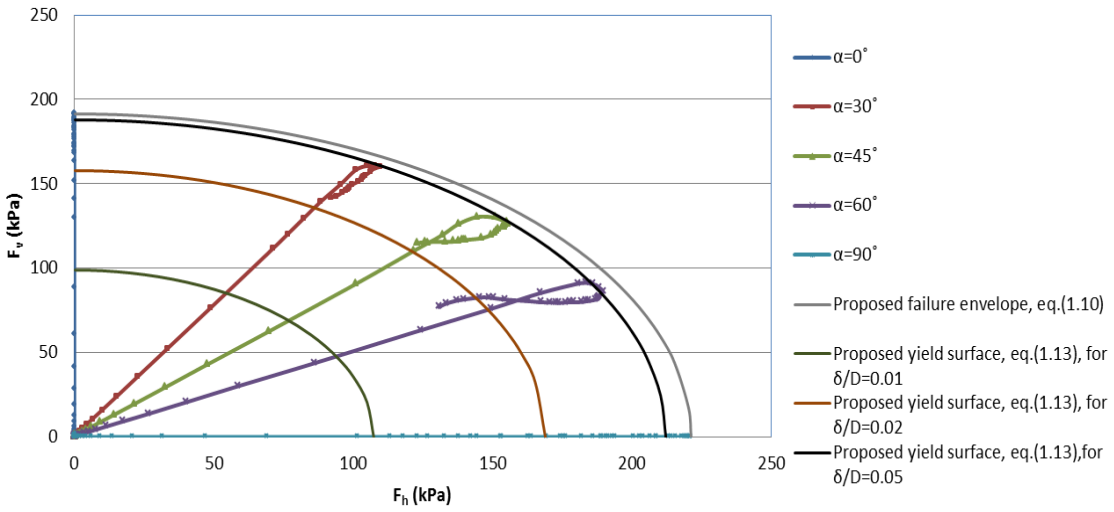

Figure 10 Mobilization of vertical and horizontal resistances in clay for pipe displacement of δ/D=0.2 in different displacement angles (α), H/D=3.03, C_u=35 kPa

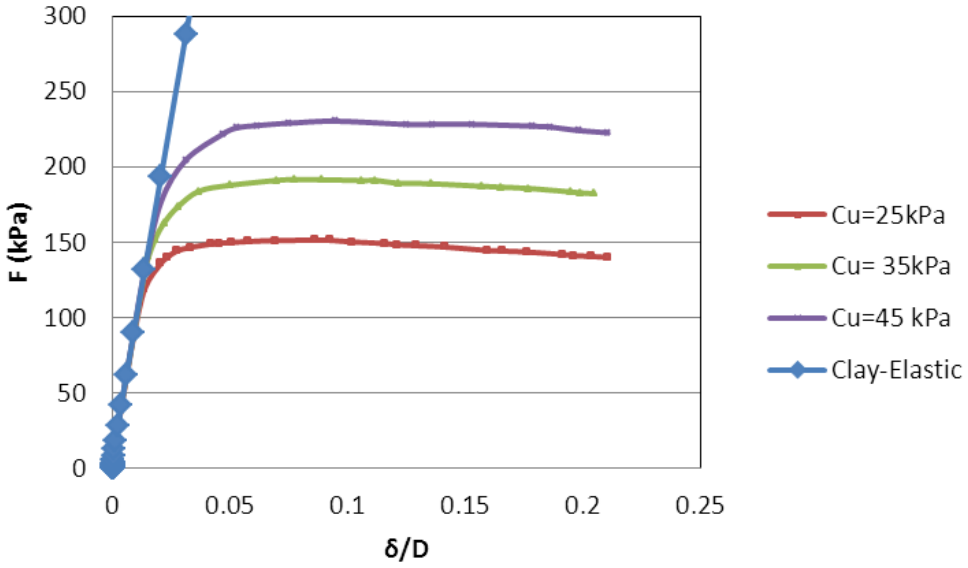

Figure 11. Normalized force-displacement curves for clay with different cohesion for H/D=3.03 and α=0

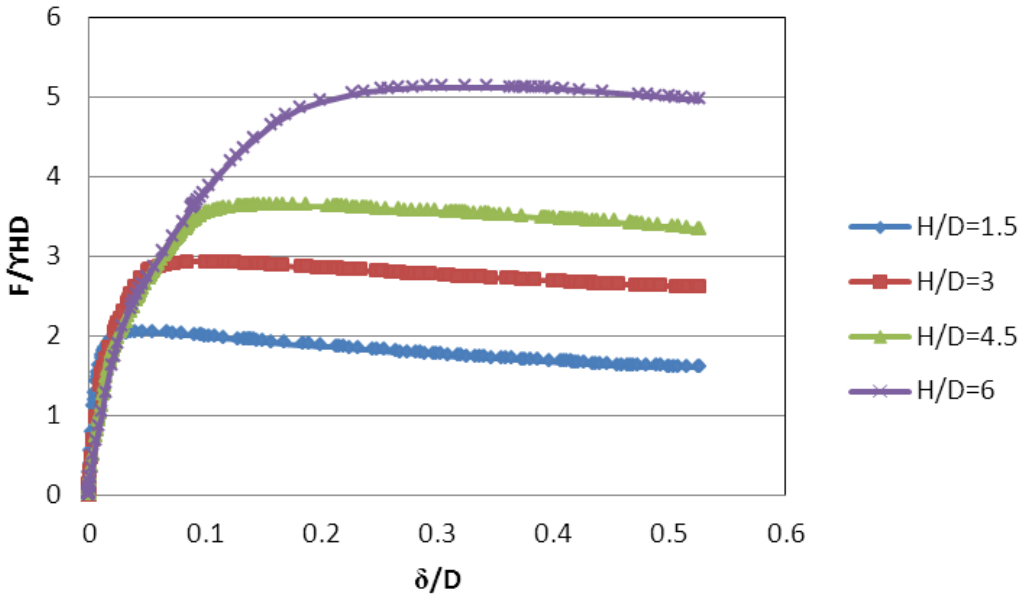

Figure 12.Effect of pipe burial depth on force-displacement response in sand for φ=35°, Ψ=10°and α=0

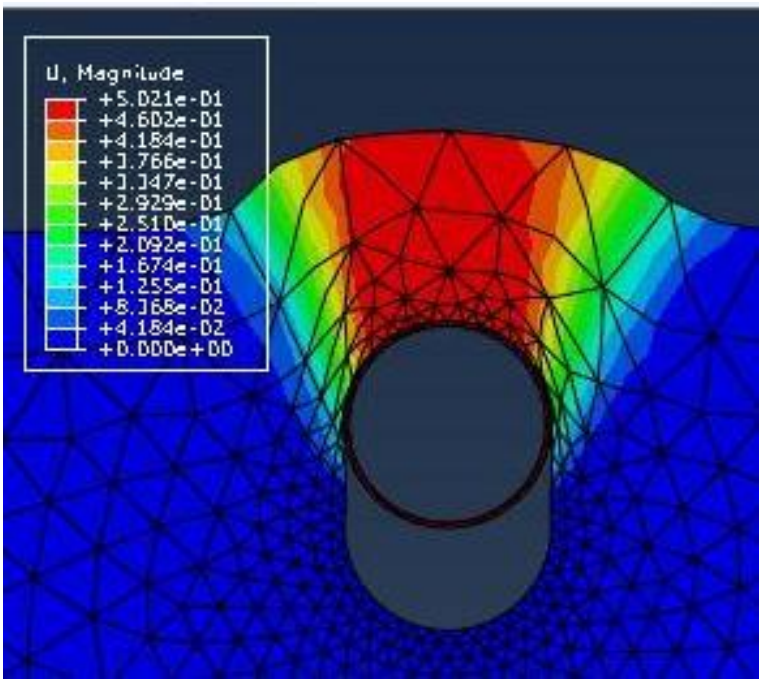

Figure 13. Deformed finite element mesh as a result of pipe vertical displacement of δ/D=0.5, α=0°, H/D=1.5, φ=35°, and Ψ=10°; Total displacement contours (m)

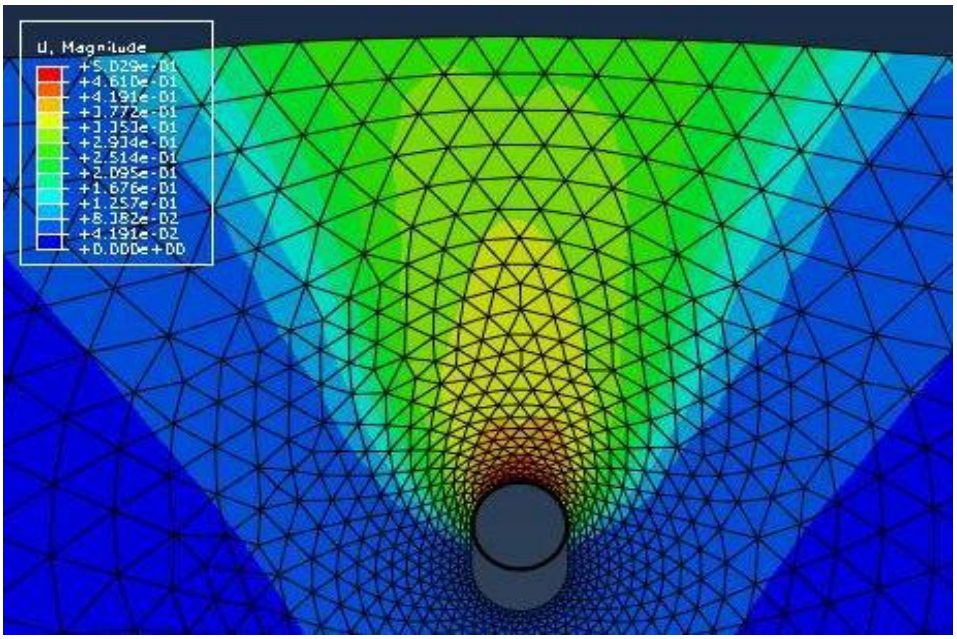

Figure 14. Deformed finite element mesh as a result of pipe vertical displacement of δ/D=0.5, α=0°, H/D=6, φ=35°and Ψ=10°; Displacement contours (m)

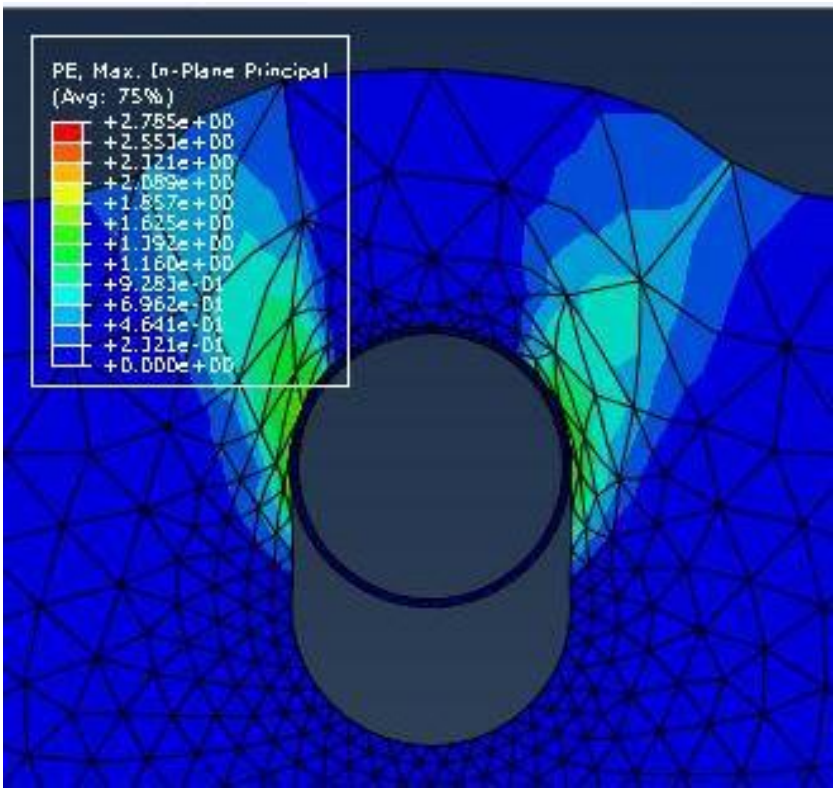

Figure 15. Deformed finite element mesh showing the plastic zone developed in sand as a result of pipe vertical displacement of δ/D=0.5, H/D= 1.5, φ=35°and Ψ=10°. Plastic strain contours (%).

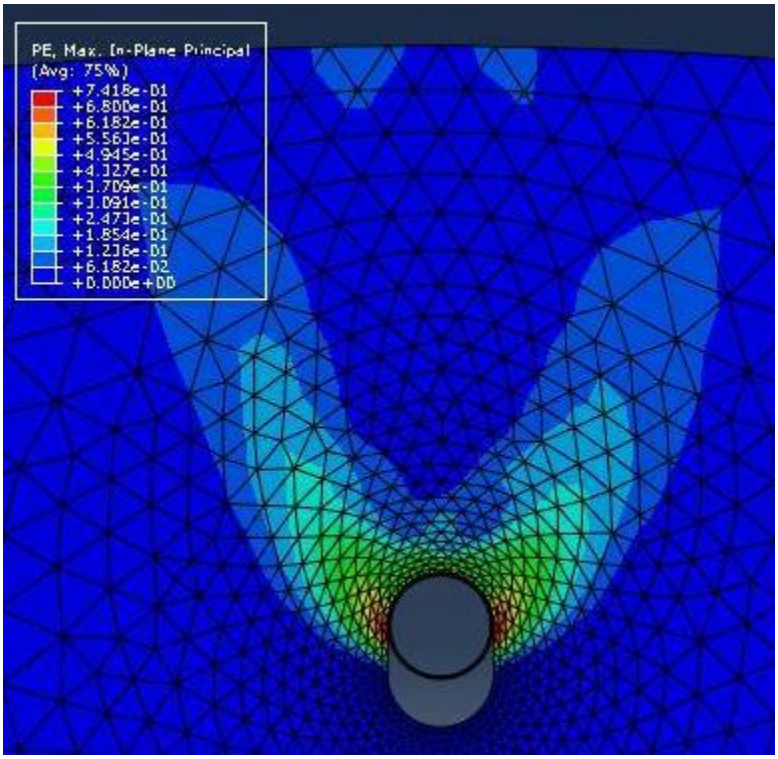

Figure 16. Deformed finite element mesh showing the plastic zone developed in sand as a result of pipe vertical displacement of δ/D=0.5, H/D= 6, φ=35°and Ψ=10°. Plastic strain contours (%)

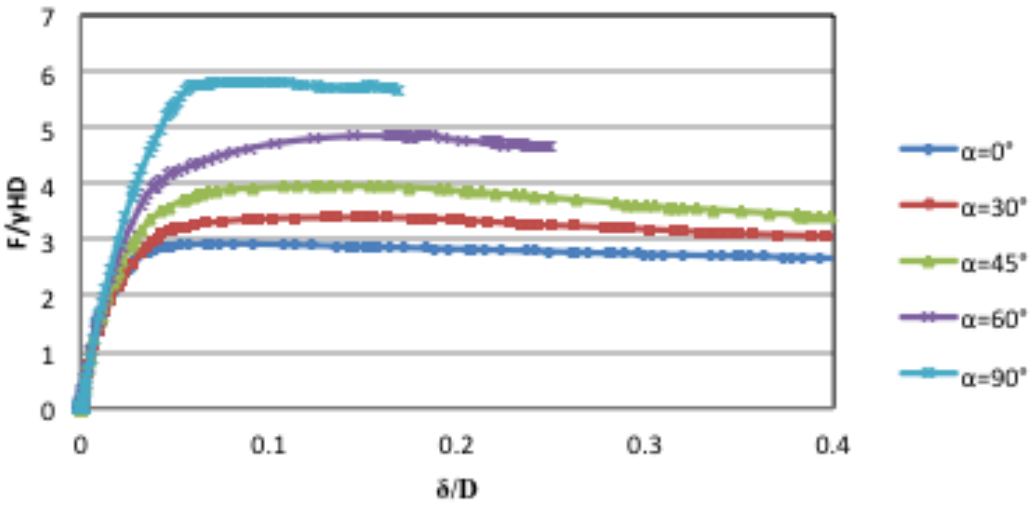

Figure 17. Effect of pipe displacement angle on force-displacement response in sand for H/D=3.03, φ=35°and Ψ=10°

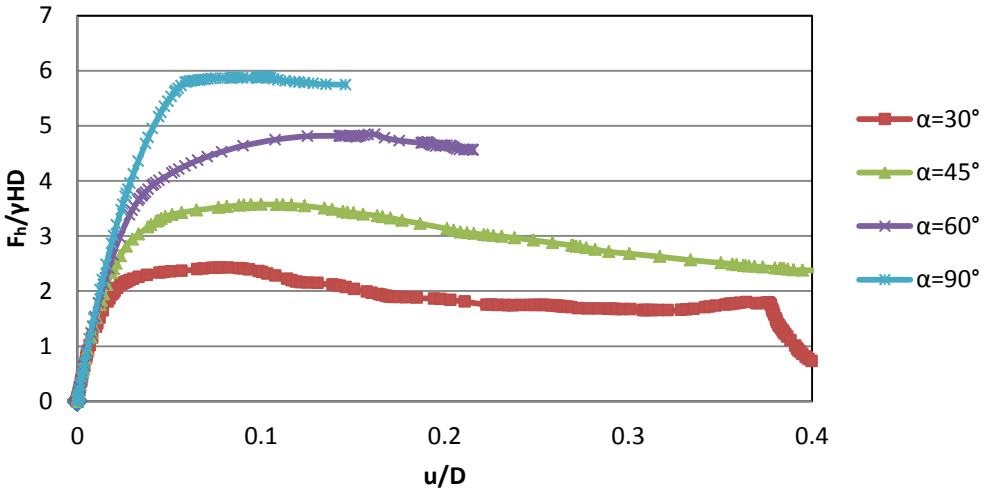

Figure 18. Effect of displacement angle on sand horizontal force-displacement response in sand for H/D=3.03, φ=35°and Ψ=10°

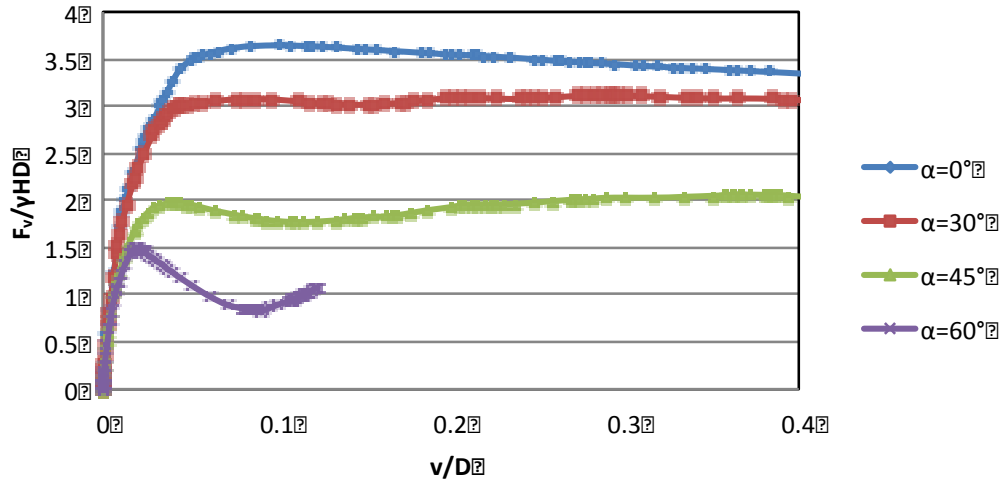

Figure 19.Effect of loading angle on sand vertical force-displacement response in sand for H/D=3.03, φ=35°and Ψ=10°

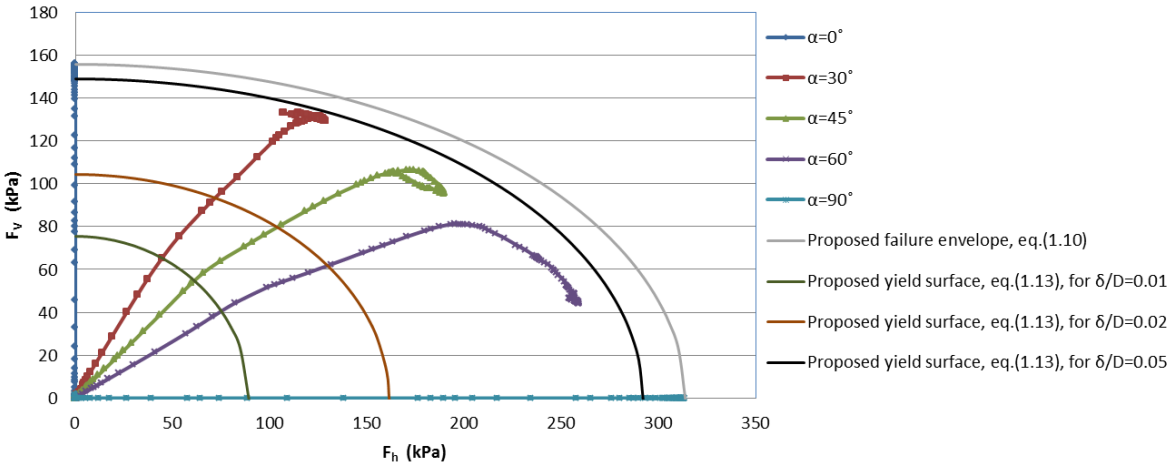

Figure 20. Sand vertical resistances versus horizontal resistance, H/D=3.03, φ=35°, Ψ=10°

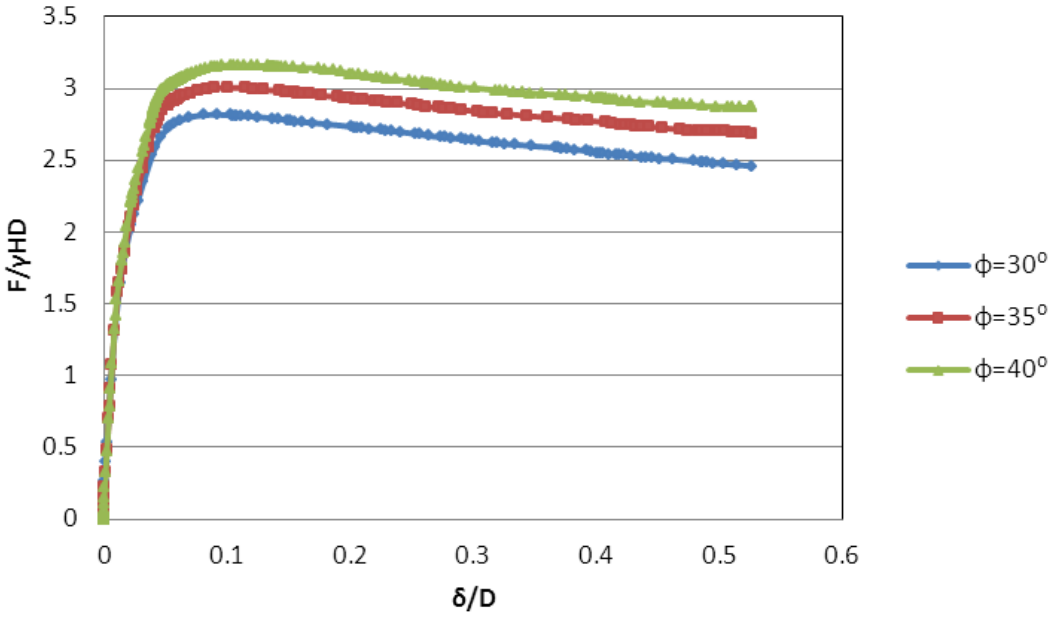

Figure 21. Effect of friction angle on force-displacement response in sand for H/D=3.03, Ψ=10°and α=0°

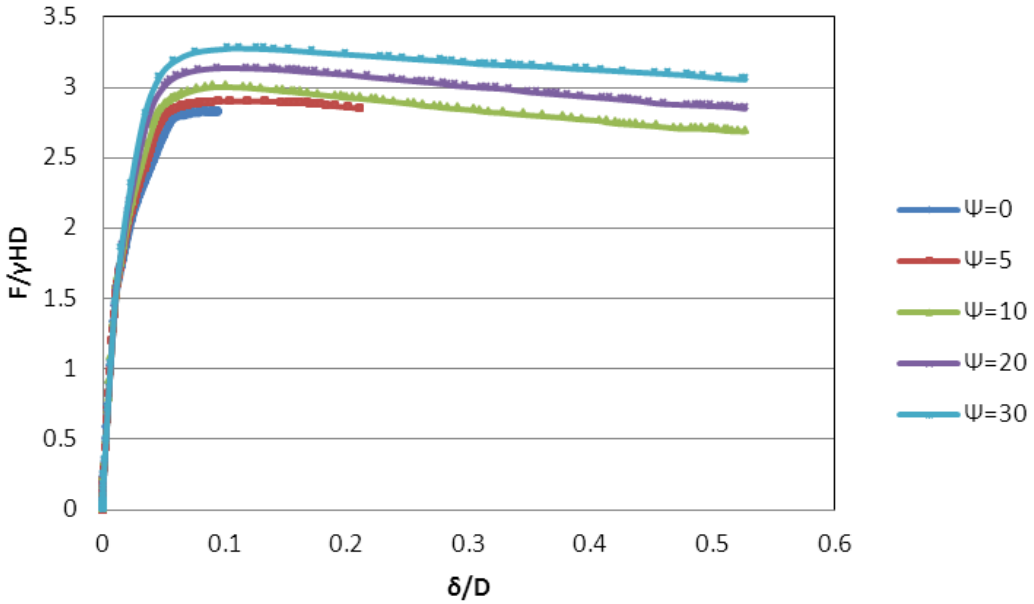

Figure 22. Effect of soil dilation angle on force-displacement response in sand for H/D=3.03, φ=35°and α=0°

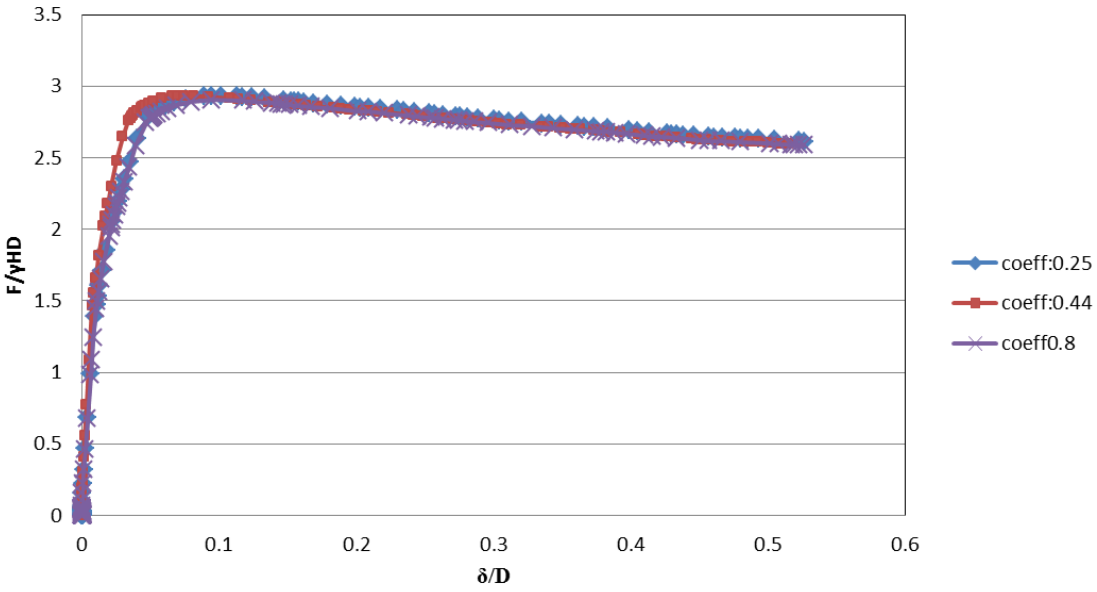

Figure 23. Effect of pipe-soil interface friction on force-displacement response in sand for H/D=3.03, φ=35°, Ψ=10°and α=0°

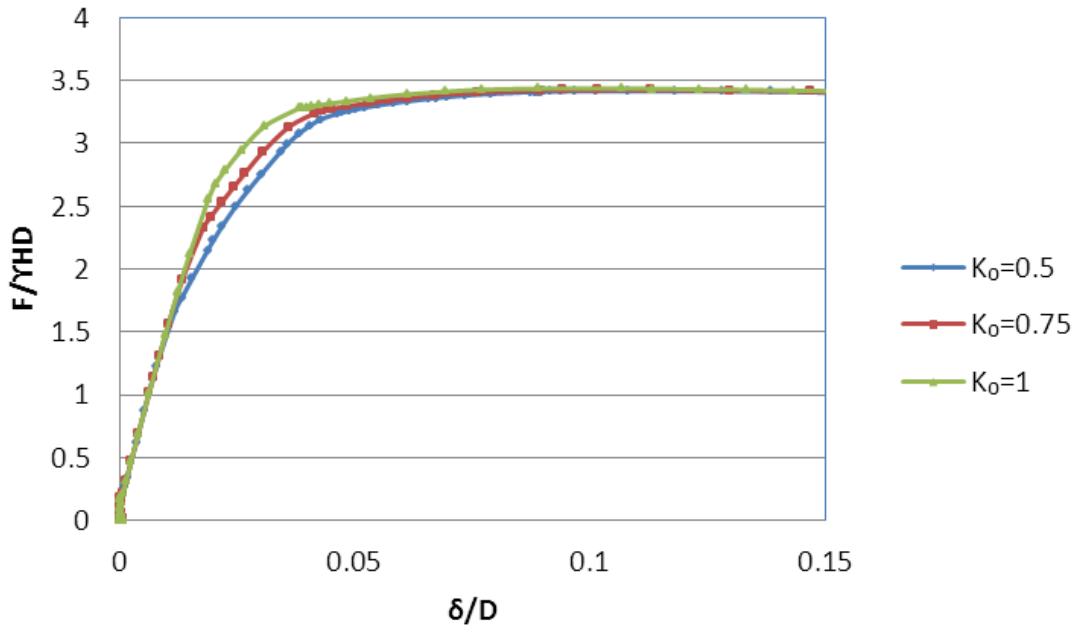

Figure 24. Effect of K_o on sand force-displacement response, H/D=3.03, ϕ=35°, Ψ=20°, α=0°

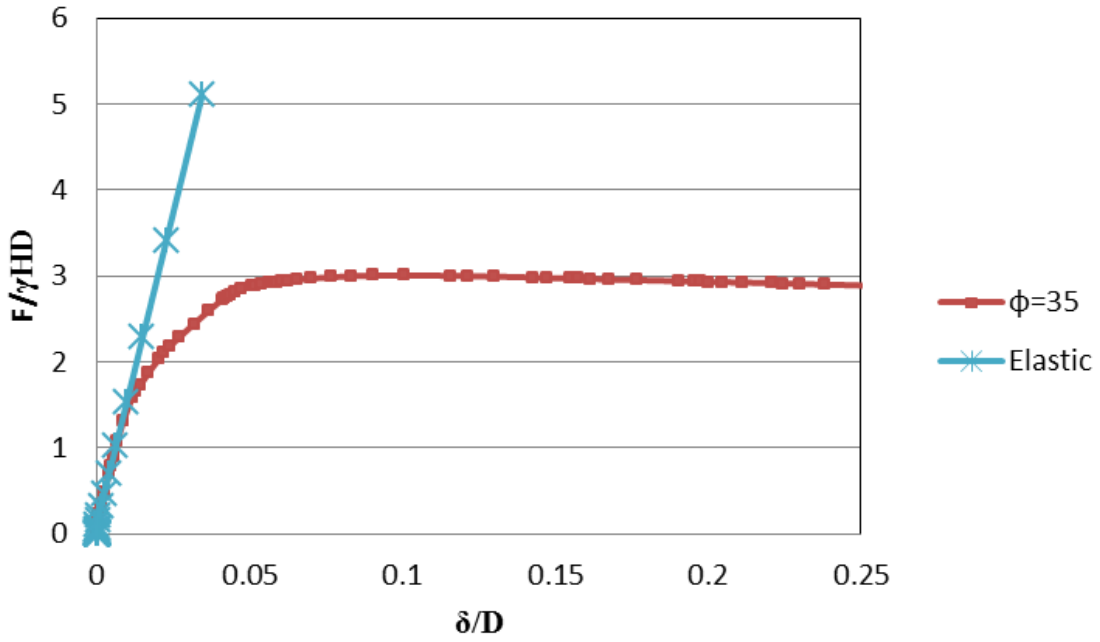

Figure 25. Force-displacement response in elastic and elasto-plastic models, H/D=3.03, α=0°

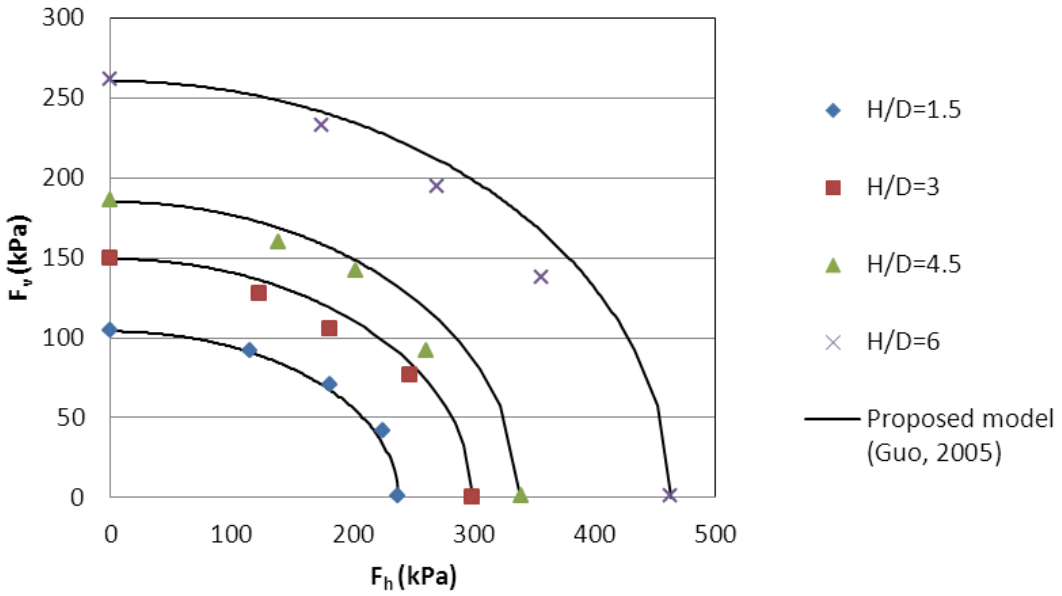

Figure 26. Failure envelope obtained from FEM analysis for different burial depth, compared to the proposed model by Guo (2005a) for ϕ=35°, Ψ=10°

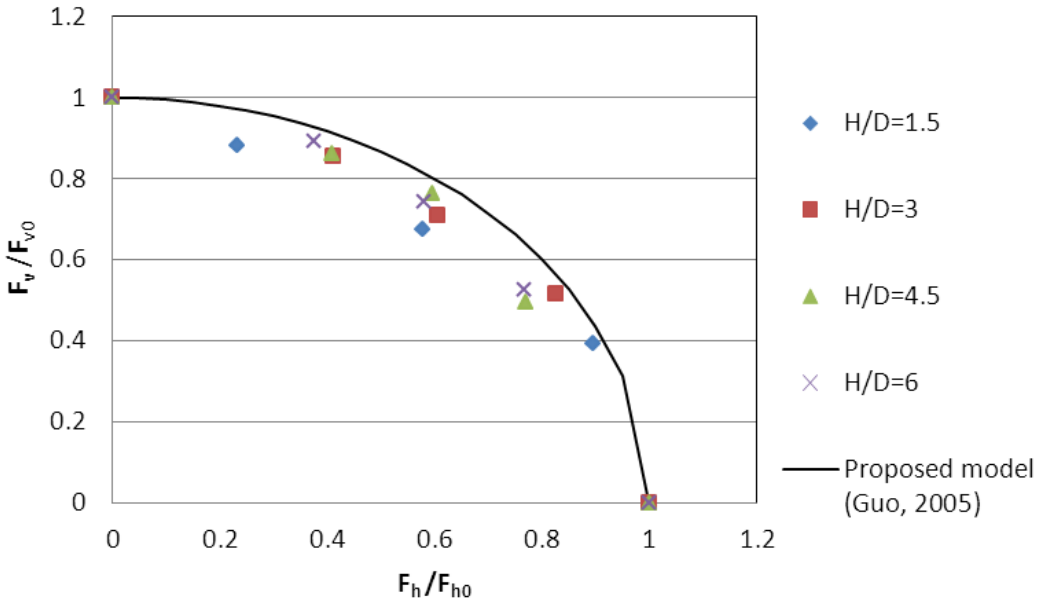

Figure 27. Failure envelope obtained from finite element normalized results for different burial depth, compared to the proposed model by Guo (2005a) for ϕ=35°, Ψ=10°

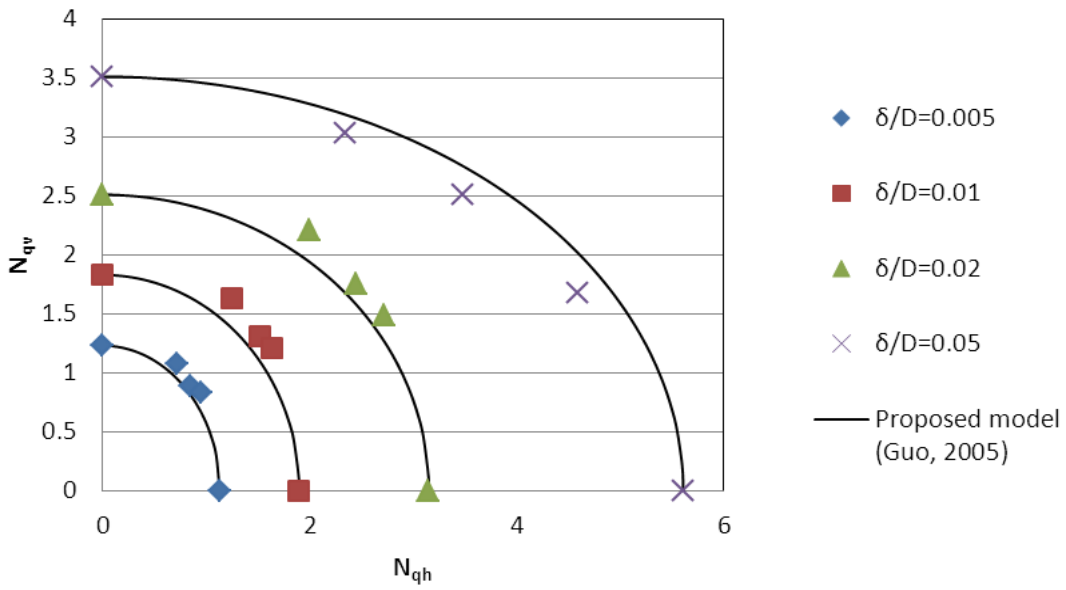

Figure 28. Yield surfaces obtained from FEM analysis for different loading surfaces, compared to the proposed model by Guo (2005a), H/D=3.03, ϕ=35°, Ψ=10°

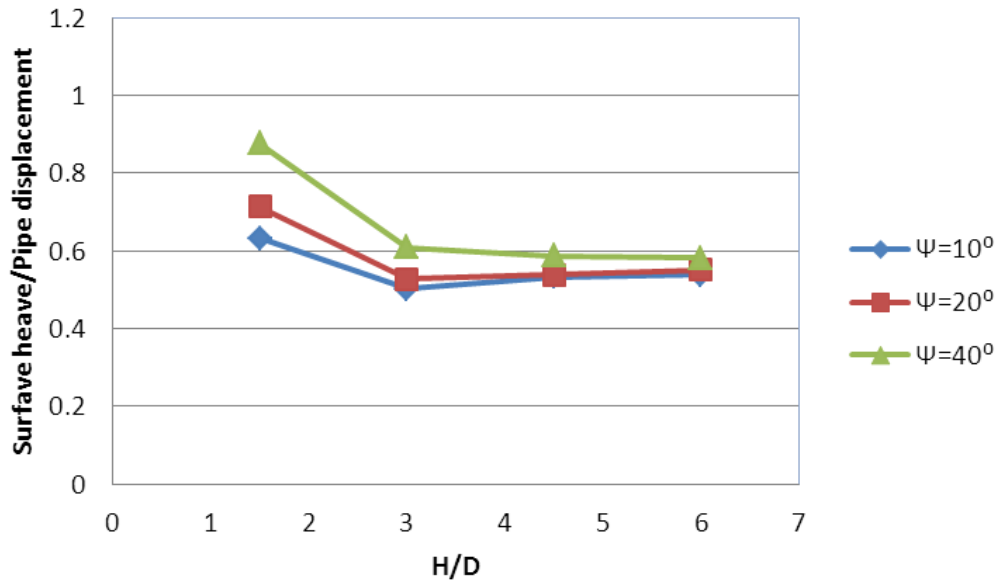

Figure 29. Effect of dilation angle and pipe burial depth on surface heave in sand for pipe vertical displacement (α=0°) and φ= 35°

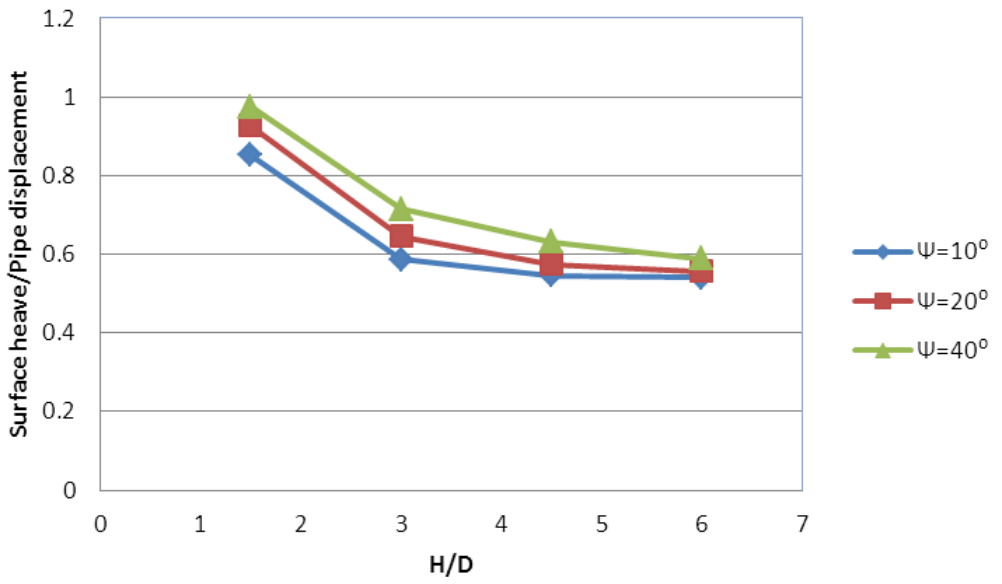

Figure 30. Effect of dilation angle and pipe burial depth on surface heave in sand for pipe 45° displacement (α=45°) and φ= 35°

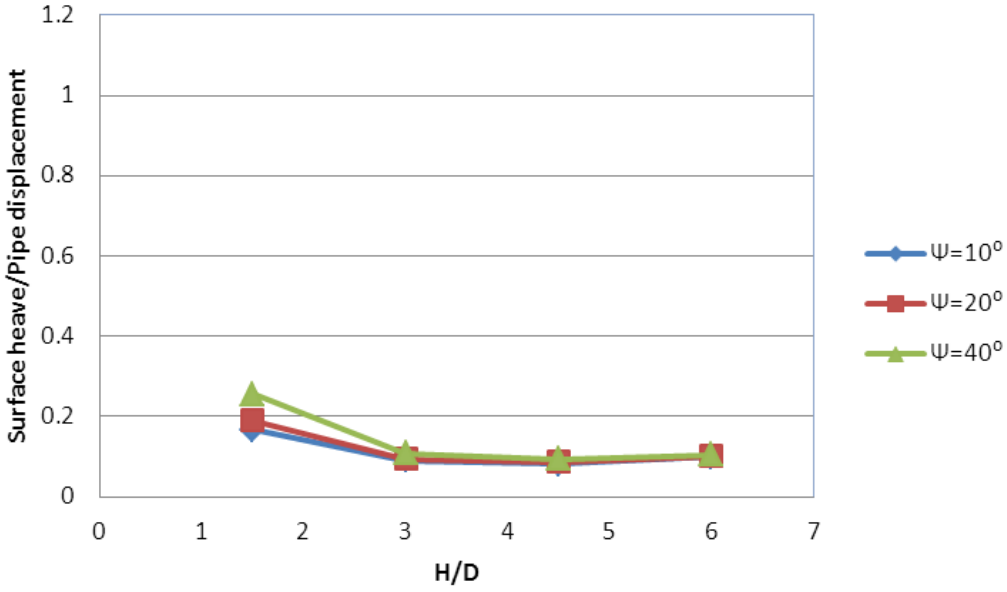

Figure 31.Effect of dilation angle and pipe burial depth on surface heave in sand for horizontal pipe displacement (α=90°) and, φ= 35°

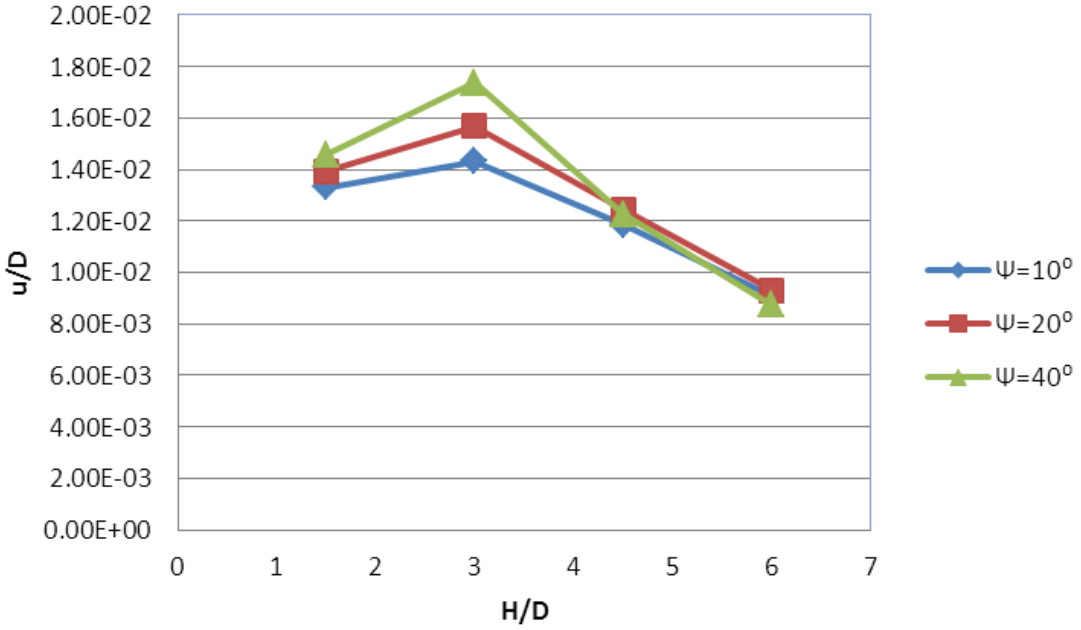

Figure 32. Effect of dilation angle and pipe burial depth on surface horizontal displacement in sand for pipe displacement of 45° (α=45°), and φ= 35°

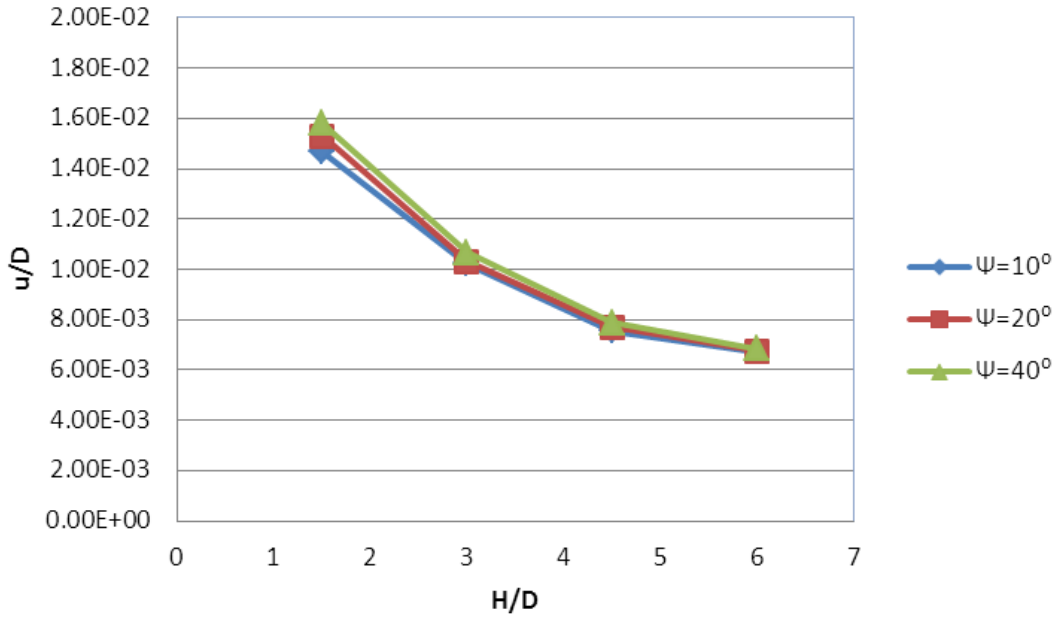

Figure 33. Effect of dilation angle and pipe burial depth on surface horizontal displacement in sand for pipe horizontal displacement (α=90°), and φ= 35°

Chapter four: Conclusion

4.1 Conclusion

In this project, the effect of soil parameters on the soil maximum resistance has been studied using finite element modeling, while the pipe is subjected to varying displacement angles.

The proposed failure envelope (Guo, 2005a) has been compared to the results from the finite element model. The comparison indicates agreement between the finite element model and the proposed failure envelope for both cohesive and frictional soils.

Also, the maximum soil resistances calculated from the finite element modeling have been compared to those predicted from ALA guideline. In general the results are in the same range obtained from the finite element analysis. In most conditions the results estimated from ALA (2001) are more conservative comparing to those calculated from the finite element modeling, except for the shallow pipes ($H/D<2$), zero dilation angle and high friction angles where the finite element modeling provides more conservative results. Since the dilation angle, pipe-soil interaction and in-situ stress have not been considered in ALA equations, for using the guideline a safety factor is needed. Based on the results from finite element modeling, a safety factor needs to be applied to the results predicted by ALA to have accurate and conservative results in pipe-soil design.

At the end, the effects of soil parameters such as dilatancy, friction angle, in-situ stress coefficient, the pipe-soil friction coefficient, and the pipe burial depth ratio on the soil maximum resistance have been investigated. The results show that the maximum normal force per unit length depends on the type of soil surrounding the pipe. By

comparing all the results pipe burial depth, soil cohesion, friction and dilation angles were found to have a significant effect on pipe-soil interaction and can considerably increase the maximum soil resistance.

The effects of the in-situ stress coefficient and pipe-soil friction coefficient on the soil maximum resistance are of less importance. By changing the pipe-soil friction coefficient, the maximum soil resistance changes less than 1%, which indicates the negligible effect of pipe roughness on the soil maximum resistance with any pipe displacement angle. Also by increasing the in-situ stress coefficient of soil from 0.5 to 1, the maximum soil resistance increases 1.5% which can be negligible.

In addition, results indicate that the larger pipe displacement angle (α) will result in a higher soil maximum resistance and as a result a pipe-soil interaction subjected to a horizontal pipe displacement ($\alpha=90°$) exhibit higher collapse loads.

The FEM results also indicate that by increasing the pipe burial depth, the surface heave and pipe horizontal displacement become independent of soil dilation angle.

4.2 Recommendation for further studies

There are several more parameters affecting pipe-soil interaction which was not considered in this project, such as soil porosity, water content, and soil creep behavior. It is recommended to consider the effect of pore water pressure on pipe-soil interaction in future studies.

Also, further studies are required to validate the model using data from experiments on pipe-soil interactions under pipe oblique displacement.

References

Achmus, A., Abdel-Rahman, Kh. (2005). Numerical modeling of vertical piles in clay under inclined compression loading. *Frontiers in Offshore Geotechnics* (pp. 391-396). Perth, Australia: Taylor & Francis.

Allotey, N., & El Naggar, M. (2008). Generalized dynamic Winkler model for nonlinear soil-structure interaction analysis. *Canadian Geotechnical Journal, 45*(4), 560-573.

Al-Mhaidib, A. (2005). Shearing rate effect on interfacial friction between sand and steel. *The fifteenth International Offshore and Polar Engineering Conference. 2*, pp. 633-640. Seoul, Korea: The Internation Society of Offshore and Polar Engineers (ISOPE).

Audibert, J.M.E, Nyman, K.J. (1977). Soil restraint against horizontal motion of pipes. *ASCE Journal of Geotechnical Engineering Division, 103*(10), 1119-1142.

Badv, K., Daryani, K.E. (2010). An investigation into the upward and lateral soil-pipeline interaction in sand using finite difference method. *Iranian Journal of Science amd Technology,Transaction B: Engineering, 34*(4), 433-445.

Cai, G., Liu, S., Puppal, A., Tong, L. (2011). Assessment of the coefficient of lateral earth pressure at rest (Ko) from in situ seismic tests. *ASTM Geotechnical Testing Journal, 34*(4), 310-320.

Canadian Geotechnical Society. (1992). *Canadian Foundation Engineering Manual.* Vancouver: The Canadian Geotechnical Society.

Carrier, W. (2005). Pipeline supported on a nonuniform Winkler soil model. *Geotechncial and Geoenvironmental Engineering, 131*(10), 1301-1304.

Daiyan, N., Kenny, S., Phillips, R., Popescu, R. (2011). Investigating pipeline-soil interaction under axial-lateral relative movements in sand. *Canadian Geotechncial Journal, 48*(11), 1683-1695.

Daiyan, N., Kenny, S., Phillips, R., Popsecu, R. (2010). Investigation of axial/lateral interacion of pipes in dense sand. *Physical modeling in Geotechnics. 1*, pp. 619-624. Zurich, Switzerland: CRC Press.

Das, B. (1985). Resistance of shallow inclined anchors in clay. Uplift behavior of anchor foundations in soil. *ASCE. 1*, pp. 86-101. New York: S. M. Clemence, ed.

Debasis, D. (2006). *Fintie element method: concepts and applications in geomechanics.* New Dehli: Prentice-Hall of India Private Limited.

Guo, P. (2005a). Numerical modeling of pipe-soil interaction under oblique loading. *Journal of Geotechnical and Geoenvironmental Engineering, 131*(2), 260-268.

Guo, P., Stolle, D. (2005b). Lateral pipe-soil inetraction in sand with reference to scale effect. *Journal of Geotechnical and Geoenvironmental Engineering, 131*(3), 338-349.

Hobbs, B.E, Ord, A., Marone, C. (1990). Dynamic behavior of rock joints. *International Society of Rock Mechanics. 1*, pp. 435-445. Leon, Norway: A.A.Balkema.

Leonards, G. (1965). *Experimental study of static and dynamic friction between soil and typical construction materials.* New Mexico: Air force weapons laboratory.

Liu, R., Li,B., Wang, H., Zhang, J., Xu, Y. (2011). Studies of soil resistance for buried pipeline uplift in sand. *Rock and Soil Mechanics, 32*(1), 27-32.

Merifield, R., White, D.J, Randolph, M.F. (2008). The ultimate undrained resistance of the partially embedded pipelines. *Geotechnique, 58*(6), 461-470.

Merifield, R.S, White, D.J, Randolph, M.F. (2009). The effect of pipe-soil interface conditions on the undrained breakout resistance of partially-embedded pipelines. *Journal of Geotechnical and Geoenvironmental Engineering, 136*(6), 819-829.

Meyerhof, G. G., Hanna, A. M. (1978). Ultimate bearing capacity of foundation on layered soil under inclined load. *Canadian Geotechnical Journal, 15*(4), 565–572.

National Energy Board. (2009). *Focus on safety and environment, a comparative analysis of pipeline performance.* Canada: The Publication Office, National Energy Board.

Nyman, K. (1984). Soil response against the oblique motion of pipes. *ASCE Journal of Transportation Engineering, 110*(2), 190-202.

Pipeline&Hazardous Materials Safety Administration. (2013). *Significant pipeline incidents*. Retrieved from U.S. Department of Transportation: http://primis.phmsa.dot.gov/comm/reports/safety/SigPSI.html?nocache=4790#_all

Rizkalla, M., Trigg, A., Simmonds, G. (1996). Recent advances in the modeling of longitudinal pipeline/soil interaction for cohesive soils. *15th International Conference on Offshore Mechanics and Arctic Engineering. 1*, pp. 325-332. ASME.

Rowe, R.K, Davis, H. (1982). The behavior of anchor plate in sand. *Geotechnique, 32*(1), 25-41.

Taylor, D. (1948). *Fundamentals of Soil mechanics.* New York: Wiley.

Trautmann, C.H, O'Rourke, T.D. (1985). Lateral force-displacement response of buried pipe. *Geotech Engineering, 111*(9), 1077-1092.

Winkler, E. (1867). *Die lehre von elastizitat und festigkeit (Teaching on elasticity and stiffness).* Prague, Czechoslovakia.

Yu, H.-S. (2006). *Plasticity and geotechncis.* Springer Science.

Zhand, X., Han, A., Wu, Z. (2011). Research on pipe-soil displacement transefr coefficient for buried pipeline. *Advanced Materials Research, 201*, 201-203.

Appendix A: Symbols

f: Failure envelope

fy: Yield function

g: Plastic potential function

C_u: undrained shear strength

D: Pipe diameter

F: Soil total bearing capacity

F_h: Soil horizontal bearing capacity (calculated from finite element modeling)

F_v: Soil vertical bearing capacity (calculated from finite element modeling)

F_{h0}: Maximum force corresponding to purely horizontal pipe movement

F_{vo}: Maximum force corresponding to purely vertical pipe movement

H: Pipe burial depth

K: Foundation modulus

K_0: Co-efficient of earth pressure at rest

N_{ch}: Clay horizontal bearing capacity factor

N_{cv}: Clay vertical bearing capacity factor

N_{qv}: Sand vertical bearing capacity factor

N_{qh}: Sand horizontal bearing capacity factor

P_u: Soil maximum horizontal resistance

Q_u: Soil maximum vertical resistance

u: Horizontal displacement

v: Vertical displacement

α: Inclination angle

ϒ : Density

δ: Total displacement

φ: Friction angle

ψ: Dilation angle

$\dot{\boldsymbol{\lambda}}$: Plastic multiplier

$\mathbf{C}^{\mathbf{e}}$: Total Stress increment tensor

ε̇: Total stress increment tensor

Appendix B: Lateral Bearing Capacity Factor of Soil (ALA2001)

Factor	φ°	a	b	c	d	e
N_{ch}	0	6.752	0.0065	-11.063	7.119	
N_{qh}	20	2.399	0.439	-0.03	$1.059x10^{-3}$	$-1.754x10^{-5}$
N_{qh}	25	3.332	0.839	-0.090	$5.606x10^{-3}$	$-1.319x10^{-4}$
N_{qh}	30	4.565	1.234	-0.089	$4.275x10^{-3}$	$-9.159x10^{-5}$
N_{qh}	35	6.816	2.019	-0.146	$7.651x10^{-3}$	$X1.683x10^{-4}$
N_{qh}	40	10.959	1.783	0.045	$-5.425x10^{-3}$	$-1.153x10^{-4}$
N_{qh}	45	17.658	3.309	0.048	$-6.443x10^{-3}$	$-1.299x10^{-4}$